XY-spin fluids in an external magnetic field: An integral equation approach

I. P. Omelyan,[1,2] W. Fenz,[2] I. M. Mryglod,[1,2] and R. Folk[2]
[1]*Institute for Condensed Matter Physics, 1 Svientsitskii Street, UA-79011 Lviv, Ukraine*
[2]*Institute for Theoretical Physics, Linz University, A-4040 Linz, Austria*
(Received 13 May 2005; published 16 September 2005)

We develop an integral equation approach to study anisotropic fluids with planar spins in the presence of an external field. As a result, the integral equation calculations for these systems appear to be no more difficult than those for ordinary isotropic liquids. The method presented is applied to the investigation of phase coexistence properties of ferromagnetic *XY*-spin fluids in a magnetic field. The soft mean spherical approximation is used for the closure relation connecting the orientationally dependent two-particle direct and total correlation functions. The Lovett-Mou-Buff-Wertheim and Born-Green-Yvon equations are employed to describe the one-particle orientational distribution. The phase diagrams are obtained in the whole range of varying the external field for a wide class of *XY*-spin fluid models with various ratios of the strengths of magnetic to nonmagnetic Yukawa-like interactions. The influence of changing the screening radii of the interaction potentials is also considered. Different types of the phase diagram topology are identified. They are characterized by the existence of critical, tricritical, critical end, and triple points related to transitions between gas, liquid, and para- and ferromagnetic states, accompanied by different external field dependencies of critical temperatures and densities corresponding to the gas-liquid and liquid-liquid transitions. As is demonstrated, the integral equation approach leads to accurate predictions of the complicated phase diagram behavior which coincide well with those evaluated by the cumbersome Gibbs ensemble simulation and multiple-histogram reweighting techniques.

DOI: 10.1103/PhysRevE.72.031506 PACS number(s): 64.70.Fx, 05.70.Fh, 64.60.−i, 75.50.Mm

I. INTRODUCTION

Spin fluids are examples of many-body systems showing a rich variety of phases in the global phase diagram [1–7]. For these systems, besides gas-liquid, liquid-liquid, and paramagnetic-ferromagnetic phase transitions, critical, tricritical, critical end, and triple point behavior can be observed. Under special conditions, an unsymmetrical tricritical van Laar point may appear also [8]. Such a complexity with respect to simple liquids arises due to the existence of additional spin degrees of freedom and the coupling between them and spatial coordinates. Moreover, the presence of spin interactions and external fields destroys the orientational homogeneity of the fluid leading to a nonuniformity or anisotropy in the distribution functions.

The properties of spin fluids have been investigated using mean field (MF) theories [1–7], integral equation (IE) approaches [8–14], as well as Monte Carlo (MC) simulation techniques [7,9,12,17–21]. Different types of models, such as the well-recognized discrete one-dimensional (1D) spin Ising, or continuous 2D spin-*XY* and 3D Heisenberg fluids, have been considered. Despite these extensive studies, the question concerning the global phase diagram topology of the *XY*-spin fluid including the influence of an external magnetic field has never been addressed. Recently, the differences in the external field dependence of critical temperatures and densities for the above three models have been identified [7]. However, the calculations were performed within a MF approach and exclusively for simplified (ideal) spin fluids, where nonmagnetic attractive interactions are absent. The more accurate IE theory has been restricted either to ideal and nonideal Ising systems [8] or to ideal Heisenberg fluids [9–14].

Surprisingly, up to recently there have been no attempts at developing the IE approach for the *XY*-spin-fluid model. This model may play a crucial role in the description of superfluid transitions in pure ^{4}He and its mixtures in bulk or in media such as porous gold [22] or silica aerogel [23]. It is generally believed [23] that the superfluid transition in ^{4}He belongs to the classical 3D *XY* model universality class (here 3D relates to the dimensionality of spatial coordinates). Similar phase diagrams are found in symmetric binary mixtures [24–31] with their gas-liquid and demixing transitions, spin lattice gas models [32,33], mixtures of ^{3}He-^{4}He with the superfluid and demixing states [22,34,35], etc. On the other hand, the fluid of particles with embedded *XY* spins described by classical statistical mechanics can be treated as one of the simplest models of disordered continuum systems exhibiting ferromagnetic behavior.

The presence of external fields produces an inhomogeneity in spin fluids characterized by an anisotropy of the one-body density. Within the standard IE approach this leads to the necessity of carrying out very complicated joint calculations for one- and two-body distribution functions on the basis of the coupled set of the anisotropic Ornstein-Zernike (AOZ) equation, a proper closure relation, and the first equation of the Born-Green-Yvon (BGY) hierarchy [36] or its Lovett-Mou-Buff-Wertheim (LMBW) counterpart [37,38]. Such calculations result in unresolvable numerical difficulties because of the restricted capabilities of even supercomputers. It is worth emphasizing also that existing IE developments for Ising [8] and Heisenberg [9–14] systems are not applicable to the *XY* fluid. The reason is that neither can it be mapped onto a binary nonmagnetic mixture (as for Ising) nor can its anisotropic correlations be expanded in spherical har-

monics (as for Heisenberg). Systems with partially constrained molecule orientations [15] also cannot be reduced to the *XY* fluid model. The specific *XY*-spin interactions require a separate IE consideration.

Quite recently [16], we have proposed a method allowing us to overcome the difficulties of the AOZ approach in the case of *XY* fluids. As has been demonstrated, the phase diagrams can readily be evaluated by expanding the one- and two-body correlation functions in terms of planar harmonics. The consideration however has been performed exclusively within the BGY scheme for the one-body distribution function and has been restricted to a particular case when the screening radii of the magnetic and nonmagnetic potentials are fixed and equal.

In this paper we develop the AOZ integral equation approach for *XY* fluids by presenting a more extended derivation of the planar harmonics expansion procedure including the LMBW scheme for the one-body correlation function. Comparison of the obtained IE solutions with our MC simulation results has shown a quantitative reproduction of the phase diagrams in a wide region of density, temperature, external field, and parameters of the interaction potentials. The dependencies of the critical temperatures and densities on the external field are presented and analyzed in detail as well. The paper is organized as follows. The *XY* model potentials, basic equations of the AOZ approach, and the conditions of phase separations are given in Sec. II. A way of providing the thermodynamic self-consistency is discussed there too. Details of the AOZ computations and MC simulations as well as the results are described and compared in Sec. III. Concluding remarks and comments are highlighted in Sec. IV.

II. INTEGRAL EQUATION APPROACH

A. The *XY*-spin-fluid model

The full potential energy of the *XY*-spin-fluid system can be written in the form

$$U=\sum_{i<j}^{N}[\phi(r_{ij})-I(r_{ij})-J(r_{ij})\mathbf{s}_i\cdot\mathbf{s}_j]-\mathbf{H}\cdot\sum_{i=1}^{N}\mathbf{s}_i, \tag{1}$$

where N is the total number of particles, $\mathbf{r}_i$ is the 3D spatial coordinate of the ith body carrying planar spin $\mathbf{s}_i$ of unit length, $r_{ij}=|\mathbf{r}_i-\mathbf{r}_j|$ denotes the interparticle separation, and $\mathbf{H}$ is the external magnetic field vector lying like $\mathbf{s}_i$ in the *XY* plane. The exchange integral of ferromagnetic ($J>0$) interactions and the nonmagnetic attraction ($I>0$) potential can be chosen in the form of Yukawa functions,

$$J(r)=\frac{2(z_1\sigma)^2}{z_1\sigma+1}\frac{\epsilon_J\sigma}{r}\exp[-z_1(r-\sigma)],$$
$$I(r)=\frac{2(z_2\sigma)^2}{z_2\sigma+1}\frac{\epsilon_I\sigma}{r}\exp[-z_2(r-\sigma)], \tag{2}$$

where ϵ_J and ϵ_I denote the interaction intensities, σ is the size of the particles, and z_1 and z_2 are the inverse screening radii of the potentials. The nonmagnetic repulsion ϕ between particles will be modeled by a more realistic soft-core (SC) potential (shifted Lennard-Jones) [7,8],

$$\phi(r)=\begin{cases}4\varepsilon\left[\left(\frac{\sigma}{r}\right)^{12}-\left(\frac{\sigma}{r}\right)^{6}\right]+\varepsilon, & r<\sqrt[6]{2}\sigma,\\ 0, & r\geqslant\sqrt[6]{2}\sigma,\end{cases} \tag{3}$$

rather than by the hard-sphere (HS) one

$$\phi_{\mathrm{HS}}(r)=\begin{cases}\infty, & r<\sigma,\\ 0, & r\geqslant\sigma.\end{cases} \tag{4}$$

The multipliers $2(z_1\sigma)^2/(z_1\sigma+1)$ and $2(z_2\sigma)^2/(z_2\sigma+1)$, appearing in Eq. (2), have been used to make the integrals $\int_\sigma^\infty I(r)d\mathbf{r}=8\pi\epsilon_I\sigma^3$ and $\int_\sigma^\infty J(r)d\mathbf{r}=8\pi\epsilon_J\sigma^3$ independent of z_1 and z_2, respectively. The latter integrals describe the contribution of the interactions to the free energy within the usual hard-sphere MF (HSMF) theory [3]. Thus the HSMF results will not depend on z_1 and z_2 for the Yukawa potentials represented in the form of Eq. (2). At $z_1=z_2=1/\sigma$ (the case which is frequently exploited in theory and simulation), the multipliers are equal to unity and we come to the usual form for $I(r)$ and $J(r)$. Within the soft-core MF (SCMF) theory [7], a slight dependence on the screening radii will appear due to the softness of the nonmagnetic repulsion potential. Then the integrals transform to $\int_0^\infty\exp[-\beta\phi(r)]\{I,J\}(r)d\mathbf{r}=8\gamma(T,z_{1,2})\pi\epsilon_{I,J}\sigma^3$, where $\beta^{-1}=k_BT$ denotes the temperature with k_B being Boltzmann's constant, and the factor $\gamma(T,z_{1,2})$ takes into account the softness of the repulsion potentials [see Eqs. (8)–(10) of Ref. [7]]. In the case of the more accurate IE approach, a more pronounced dependence of the results on z_1 and z_2 will be observed (see Sec. III). Note that the IE theory takes into account pair correlations between particles in spin space, which are ignored within the MF approximation.

B. Standard AOZ formulation

A complete thermodynamic and magnetic description of the system considered can be performed in terms of orientationally dependent one-body $\xi(\varphi)$ and two-body $g(r,\varphi_1,\varphi_2)=h(r,\varphi_1,\varphi_2)+1$ distribution functions. The angles φ are referred to the external field, so that $\mathbf{H}\cdot\mathbf{s}=H\cos\varphi$ and $\mathbf{s}_1\cdot\mathbf{s}_2=\cos(\varphi_1-\varphi_2)$. According to the liquid state theory [36,39], the total correlation function h satisfies the AOZ equation which in our case reads

$$h(r,\varphi_1,\varphi_2)=c(r,\varphi_1,\varphi_2)+\frac{\rho}{2\pi}\int_V d\mathbf{r}'\int_0^{2\pi}d\varphi\xi(\varphi)\times c(|\mathbf{r}-\mathbf{r}'|,\varphi_1,\varphi)h(r',\varphi,\varphi_2), \tag{5}$$

where $\rho=N/V$ is the particle number density, V the volume, and $c(r,\varphi_1,\varphi_2)$ the direct correlation function (note that a positionally homogeneous and orientationally anisotropic system is being investigated).

The AOZ equation (5) must be complemented by a closure relation. The most general form of it is

$$g(r,\varphi_1,\varphi_2)=\exp[-\beta u(r,\varphi_1,\varphi_2)+h(r,\varphi_1,\varphi_2)-c(r,\varphi_1,\varphi_2)+B(r,\varphi_1,\varphi_2)], \tag{6}$$

where g denotes the radial distribution function,

$$u(r,\varphi_1,\varphi_2) = \phi(r) - I(r) - J(r)\cos(\varphi_1 - \varphi_2) \tag{7}$$

is the interparticle potential, and B the bridge function [formally setting $B=0$ corresponds to the hypernetted chain (HNC) approximation]. The bridge function cannot be determined exactly for any system of interacting particles, but a lot of approaches exist allowing one to present it approximately [36]. One of the ways is to use the soft mean spherical ansatz (SMSA) [8,40]

$$B(r,\varphi_1,\varphi_2) = \ln[1+\tau(r,\varphi_1,\varphi_2)] - \tau(r,\varphi_1,\varphi_2), \tag{8}$$

where

$$\tau(r,\varphi_1,\varphi_2) = h(r,\varphi_1,\varphi_2) - c(r,\varphi_1,\varphi_2) - \beta u_1(r,\varphi_1,\varphi_2)$$

and the long-ranged part u_1 can be extracted from the total potential u using the Boltzmann-like switching exponent built on the soft-core potential [8], i.e.,

$$u_1(r,\varphi_1,\varphi_2) = -[I(r) + J(r)\cos(\varphi_1 - \varphi_2)]\exp[-\beta\phi(r)].$$

In the particular case $\phi(r) \to \phi_{\mathrm{HS}}(r)$, we come to the usual hard-sphere MSA with $g(r,\varphi_1,\varphi_2)=0$ for $r<\sigma$ and $c(r,\varphi_1,\varphi_2)=\beta[I(r)+J(r)\cos(\varphi_1-\varphi_2)]$ at $r\geqslant\sigma$.

Evaluation of pair correlations from the AOZ equation (5) requires the knowledge of the one-body distribution function $\xi(\varphi)$. This function is obtained from the first member of the BGY hierarchy [36],

$$\frac{d}{d\varphi}\ln\xi(\varphi) = \frac{d}{d\varphi}\beta H\cos\varphi - \beta\frac{\rho}{2\pi}\int_V d\mathbf{r}\int_0^{2\pi} d\varphi' \times \xi(\varphi')g(r,\varphi,\varphi')\frac{du(r,\varphi,\varphi')}{d\varphi'}. \tag{9}$$

Alternatively, the function $\xi(\varphi)$ can be evaluated using the LMBW equation [37,38]

$$\frac{\mathrm{d}}{\mathrm{d}\varphi}\ln\xi(\varphi) = \frac{\mathrm{d}}{\mathrm{d}\varphi}\beta H\cos\varphi + \frac{\rho}{2\pi}\int_V d\mathbf{r}\int_0^{2\pi} d\varphi' \times c(r,\varphi,\varphi')\frac{d\xi(\varphi')}{d\varphi'}. \tag{10}$$

The BGY and LMBW equations are equivalent and will lead to identical results, provided the anisotropic correlation functions $g(r,\varphi,\varphi')$ and $c(r,\varphi,\varphi')$ are evaluated exactly. This is, however, not the case in practical implementations, where the correlation functions are calculated approximately in view of the approximate character of the bridge function.

Equations (5), (6), (9), and (10) constitute a very complicated set of coupled AOZ-SMSA-BGY or AOZ-SMSA-LMBW nonlinear integro-differential equations with respect to h (or g), c, and ξ. The main problem in solving it is that the unknowns $h(r,\varphi,\varphi')$ and $c(r,\varphi,\varphi')$ depend on up to three (one spatial and two angle) variables (instead of one spatial coordinate as in the case of simple homogeneous liquids). This complicates the calculations drastically and leads to unresolvable numerical difficulties. Thus a method is needed to remedy such a situation.

C. Reformulation of the AOZ equation

1. Expansions in orthogonal polynomials

Any periodic function of two angle variables can be expanded in sine and cosine harmonics as

$$f(r,\varphi_1,\varphi_2) = \sum_{n,m=0}^{\infty}\sum_{l,l'=0,1} f_{nmll'}(r)T_{nl}(\varphi_1)T_{ml'}(\varphi_2) \tag{11}$$

using the orthogonal Chebyshev polynomials

$$T_{n0}(\varphi) = \cos(n\varphi), \qquad T_{n1}(\varphi) = -\frac{1}{n}\frac{dT_{n0}(\varphi)}{d\varphi} = \sin(n\varphi). \tag{12}$$

The planar expansion (11) can readily be applied to our two-body functions $\{h,g,c\}\equiv f$ with the simplification $f_{nmll'}=f_{nml}\delta_{ll'}$ because these functions are invariant with respect to the transformation $(\varphi_1,\varphi_2)\leftrightarrow(-\varphi_1,-\varphi_2)$ in view of the symmetry of Hamiltonian (1). Then exploiting the orthonormality condition

$$\int_0^{2\pi} T_{nl}(\varphi)T_{ml'}(\varphi)d\varphi = t_n\delta_{nm}\delta_{ll'}, \tag{13}$$

where $t_n=\pi(1-\delta_{n0})+2\pi\delta_{n0}$, yields the expansion coefficients

$$f_{nml}(r) = \frac{1}{t_n t_m}\int_0^{2\pi}\int_0^{2\pi} d\varphi_1 d\varphi_2 f(r,\varphi_1,\varphi_2)T_{nl}(\varphi_1)T_{ml}(\varphi_2). \tag{14}$$

Note that from the mathematical point of view, the idea of expessing functions in terms of planar harmonics [Eq. (11)] is of course not new and presents in fact a two-dimensional generalization of the well-known expansion of one-variable periodic functions on Fourier harmonics. However, the first results of its actual implementation in the context of the integral equation approach for specific *XY*-spin interactions have been shown by us in Ref. [16].

2. Mapping to an isotropic mixture

In terms of the above expansion coefficients, the AOZ equation (5) can be reduced to the form

$$h_{nml}(k) = c_{nml}(k) + \rho\sum_{n',m'} c_{nm'l}(k)\xi_{n'm'l}h_{n'ml}(k), \tag{15}$$

where

$$\xi_{nml} = \frac{1}{2\pi}\int_0^{2\pi}\xi(\varphi)T_{nl}(\varphi)T_{ml}(\varphi)d\varphi \tag{16}$$

are the angle moments of $\xi(\varphi)$, and the 3D Fourier transform $f(k)=\int_V f(r)\exp(\mathrm{i}\mathbf{k}\cdot\mathbf{r})d\mathbf{r}$ has been used. The matrix representation (15) looks like the OZ equation corresponding to a mixture of simple homogeneous fluids of nonmagnetic particles. This is a very important feature because the problem can now be solved by adapting algorithms already known for isotropic systems.

Furthermore, we perform the one-body polynomial expansion

$$\xi(\varphi) = Z^{-1} \exp\left[\beta\left(H\cos\varphi + \sum_{n=1}^{\infty} a_n T_{n0}(\varphi)\right)\right], \quad (17)$$

where only cosine harmonics appear due to the property $\xi(-\varphi)=\xi(\varphi)$ and

$$Z = \frac{1}{2\pi}\int_0^{2\pi} \exp\left[\beta\left(H\cos\varphi + \sum_{n=1}^{\infty} a_n T_{n0}(\varphi)\right)\right] d\varphi \quad (18)$$

is determined from the normalization condition

$$\frac{1}{2\pi}\int_0^{2\pi} \xi(\varphi)\, d\varphi = 1.$$

Then the cumbersome integro-differential equations (9) and (10) can be solved with respect to angle variables analytically. The results in the cases of the BGY and LMBW equations are

$$a_n = \frac{\rho}{2n}\int d\mathbf{r} \sum_{\substack{m=0 \\ l,l'=0,1}}^{\infty} (-1)^{l+l'} \xi_{m1l} g_{\tilde{n}ml}(r) J(r), \quad (19)$$

where $\tilde{n}=n-1+2l'$, and

$$a_n = \frac{\rho}{n}\sum_{m=1}^{\infty} m \int d\mathbf{r}\; c_{nm1}(r)\xi_{m00} = \frac{\rho}{n}\sum_{m=1}^{\infty} m\xi_{m00} c_{nm1}(k=0), \quad (20)$$

respectively, with $n \geqslant 1$.

Handling the SMSA closure (6) also presents no difficulties, because for distances $r \geqslant 2^{1/6}\sigma$ [where $\phi(r)=0$; see Eq. (3)] we obtain from Eqs. (6)–(8) that $c(r,\varphi_1,\varphi_2)=\beta[I(r)+J(r)\cos(\varphi_1-\varphi_2)]$. Taking into account the expansion

$$\cos(\varphi_1-\varphi_2) = T_{10}(\varphi_1)T_{10}(\varphi_2) + T_{11}(\varphi_1)T_{11}(\varphi_2), \quad (21)$$

one finds $c_{000}(r)=\beta I(r)$ and $c_{110}(r)=c_{111}(r)=\beta J(r)$, while all other c coefficients will be equal to zero at $r \geqslant 2^{1/6}\sigma$. Only for $r < 2^{1/6}\sigma$ should we perform a numerical integration [according to Eq. (14)] of the right-hand side of Eq. (6) in order to get the expansion coefficients $g_{nml}(r)$.

Another important feature of the presented approach is that only a small number $\mathcal{N}$ of harmonics should be, in fact, involved into the computations because the expansion coefficients rapidly tend to zero with increasing $\mathcal{N}$. Then the sums $\Sigma_{n,m}^{\infty}$ can be replaced without loss of precision by finite ones with $n,m \leqslant \mathcal{N}$. In our case, the anisotropic potential $u(r,\varphi_1,\varphi_2)$ is expanded in terms of zeroth and first harmonics [see Eqs. (7) and (21)] exclusively, while a slight anharmonicity ($\mathcal{N}>1$) in the correlation functions will appear due to the nonlinearity of the closure.

3. Thermodynamic and magnetic quantities

Once the expansion coefficients are found, all the magnetic and thermodynamic properties of the system are obtained in a straightforward way (except the chemical potential and free energy whose evaluation presents a nontrivial task, see Appendices A and B). Using first the standard formulas [36,39] of anisotropic fluids and then applying Eqs. (7), (11)–(14), (16), and (21) one finds, in particular, for the mean internal potential energy $\mathcal{U}$ and the isothermal compressibility $\mathcal{K}_T$ the following expressions:

$$\begin{aligned}\frac{\mathcal{U}}{N} &= \frac{1}{2}\frac{\rho}{(2\pi)^2}\int d\mathbf{r}\, d\varphi_1 d\varphi_2 \xi(\varphi_1)\xi(\varphi_2) g(r,\varphi_1,\varphi_2) \\ &\quad \times u(r,\varphi_1,\varphi_2) \\ &= \frac{\rho}{2}\sum_{n,m=0}^{\infty}\int d\mathbf{r}([\phi(r)-I(r)]\times \xi_{n00}\xi_{m00} g_{nm0}(r) \\ &\quad - J(r)\sum_{l=0,1}\xi_{n1l}\xi_{m1l} g_{nml}(r)) \end{aligned} \quad (22)$$

and

$$\begin{aligned}\rho k_B T \mathcal{K}_T &= 1 + \frac{\rho}{(2\pi)^2}\int d\mathbf{r}\, d\varphi_1 d\varphi_2 \xi(\varphi_1)\xi(\varphi_2) h(r,\varphi_1,\varphi_2) \\ &= 1 + \rho\sum_{n,m=0}^{\infty}\int d\mathbf{r}\; \xi_{n00}\xi_{m00} h_{nm0}(r) \\ &= 1 + \rho\sum_{n,m=0}^{\infty} \xi_{n00}\xi_{m00} h_{nm0}(k=0), \end{aligned} \quad (23)$$

whereas the pressure P can be calculated from the virial equation

$$\begin{aligned}\frac{\beta P}{\rho} &= 1 - \frac{1}{6}\frac{\beta\rho}{(2\pi)^2}\int d\mathbf{r}\, d\varphi_1 d\varphi_2 \xi(\varphi_1)\xi(\varphi_2) g(r,\varphi_1,\varphi_2) \\ &\quad \times r\frac{du(r,\varphi_1,\varphi_2)}{dr} \\ &= 1 - \frac{\beta\rho}{6}\sum_{n,m=0}^{\infty}\int r\, d\mathbf{r}\left(\frac{d[\phi(r)-I(r)]}{dr}\times \xi_{n00}\xi_{m00} g_{nm0}(r)\right. \\ &\quad \left. - \frac{dJ(r)}{dr}\sum_{l=0,1}\xi_{n1l}\xi_{m1l} g_{nml}(r)\right). \end{aligned} \quad (24)$$

The magnitude of the magnetization per particle is

$$M = |\mathbf{M}| = \frac{1}{N}\left|\left\langle \sum_{i=1}^{N} \mathbf{s}_i \right\rangle\right| = \frac{1}{2\pi}\int_0^{2\pi} \cos(\varphi)\xi(\varphi)\, d\varphi \equiv \xi_{100}, \quad (25)$$

where $\langle\,\rangle$ denotes the statistical averaging. The elements of the magnetic susceptibility tensor are

$$\begin{aligned}\chi_{\alpha\beta} &= \rho\frac{\partial M_\alpha}{\partial H_\beta} = \rho\beta\{\langle s_{1\alpha}s_{1\beta}\rangle - \langle s_{1\alpha}\rangle\langle s_{1\beta}\rangle + (N-1) \\ &\quad \times\langle[s_{1\alpha}-\langle s_{1\alpha}\rangle][s_{2\beta}-\langle s_{2\beta}\rangle]\rangle\}, \end{aligned} \quad (26)$$

where $\alpha,\beta=x,y$ relate to the components of vectors $\mathbf{M},\mathbf{H}$, and $\mathbf{s}_i$ which all lie in the XY plane. Fixing without loss of generality the direction of the external field vector $\mathbf{H}$ along the X axis, one gets the longitudinal

$$\chi_{xx} = \rho\beta\left(\xi_{110} - \xi_{100}^2 + \rho \sum_{n,m=0}^{\infty} \xi_{n10}\xi_{m10}h_{nm0}(k=0) \right) \quad (27)$$

and transverse

$$\chi_{yy} = \rho\beta\left(\xi_{111} + \rho \sum_{n,m=1}^{\infty} \xi_{n11}\xi_{m11}h_{nm1}(k=0) \right) \quad (28)$$

components of χ, while the off-diagonal elements $\chi_{xy}=\chi_{yx}=0$ will vanish.

The chemical potential can be written in the form

$$\mu = \mu^* + k_B T(\ln \rho + 3 \ln \Lambda), \quad (29)$$

where Λ denotes the de Broglie thermal wavelength and

$$\mu^* = -k_B T \ln Z_0 + \frac{\rho}{(2\pi)^2}\int_0^1 d\lambda \int d\mathbf{r}\, d\varphi_1 d\varphi_2 \times \xi(\varphi_1)\xi_\lambda(\varphi_2) g_\lambda(r,\varphi_1,\varphi_2)\frac{\partial u_\lambda(r,\varphi_1,\varphi_2)}{\partial\lambda} \quad (30)$$

is the excess part (see Appendix A). The excess chemical potential in turn consists of the intrinsic term related to the one-body distribution function $\xi_0(\varphi)=\exp(\beta H\cos\varphi)/Z_0$ of a noninteracting system, where $Z_0=(1/2\pi)\int\exp(\beta H\cos\varphi)d\varphi$, and the contribution arising when the interparticle interactions are taken into account. The integration over the coupling parameter λ in the last term of the right-hand side of Eq. (30) corresponds, in fact, to the computation of work needed for transferring a separate particle (whose angle coordinate is marked by φ_2) from a collection of noninteracting spins [$\lambda=0$ with $u_{\lambda=0}\equiv 0$, $g_{\lambda=0}\equiv 1$, and $\xi_{\lambda=0}(\varphi_2)\equiv\xi_0(\varphi_2)$] to the system [$\lambda=1$ with $u_{\lambda=1}\equiv u$, $g_{\lambda=1}\equiv g$, and $\xi_{\lambda=1}(\varphi_2)\equiv\xi(\varphi_2)$] in the presence of a fixed external field H. Equation (30) represents an anisotropic generalization of the well-known Kirkwood (charging) formula [41] for isotropic systems. As for isotropic systems [8,42,43], the λ integration in Eq. (30) can be performed analytically. In our case this leads to much more cumbersome computations because of the anisotropy [$\xi(\varphi_1)\neq 1$ and $\xi_\lambda(\varphi_2)\neq 1$] of the system. The results are presented in Appendix A. It has been shown there that in general μ cannot be reduced to an expression in terms of only harmonics coefficients h_{nml}, c_{nml}, or g_{nml}, ξ_{nml}, as has been done above for the other quantities [see Eqs. (22)–(28)]. In order to obtain μ, it is necessary to explicitly perform some angle integrations with the bridge function [see Eq. (A16)].

4. Phase separations

The first-order phase transitions between gas and liquid states can be determined at given values of T and H from the mechanical and chemical equilibrium conditions

$$P(\rho^{\mathrm{I}},T,H) = P(\rho^{\mathrm{II}},T,H), \qquad \mu(\rho^{\mathrm{I}},T,H) = \mu(\rho^{\mathrm{II}},T,H), \quad (31)$$

where ρ^{I} and ρ^{II} are the densities of coexisting phases I and II. While the pressure P can readily by calculated when solving Eq. (31) using the virial equation of state (24), the chemical potential evaluation requires numerical integration with respect to up to three variables r, φ_1, and φ_2 according to Eq. (A17). The only way to avoid such a time-consuming computation is to apply the thermodynamic relation $\rho\beta(\partial\mu^*/\partial\rho)_{T,H}=\beta(\partial P/\partial\rho)_{T,H}-1$ which follows from the Gibbs-Duhem equality $\mathcal{S}\,dT - V\,dP + N(d\mu - M\,dH)=0$, where $\mathcal{S}$ denotes the entropy [8,46]. Then the chemical potential can be evaluated by integrating the pressure over density as

$$\beta\mu_P^*(\rho,T,H) = \frac{\beta P}{\rho} - 1 + \int_0^\rho \frac{1}{\rho'}\left(\frac{\beta P(\rho',T,H)}{\rho'} - 1 \right) d\rho' \quad (32)$$

[note that $\beta P/\rho - 1$ is proportional to ρ according to Eq. (24), so that no singularity arises in the integrand at $\rho\to 0$]. In view of Eq. (32), the second line of Eq. (31) can be replaced by the well-known Maxwell construction

$$\left(\frac{1}{\rho^{\mathrm{II}}} - \frac{1}{\rho^{\mathrm{I}}} \right)\mathcal{P} + \int_{\rho^{\mathrm{I}}}^{\rho^{\mathrm{II}}} P(\rho,T,H)\frac{d\rho}{\rho^2} = 0, \quad (33)$$

where $\mathcal{P}$ denotes the coexistence pressure.

The paramagnetic-ferromagnetic transition of the second order has been found as a boundary Curie curve $T_\lambda(\rho)$ in the temperature-density plane, where nonzero (spontaneous) magnetization $M\neq 0$ becomes possible at $H=0$. Below this curve, i.e., for $T<T_\lambda(\rho)$, we will have a nontrivial solution for the expansion coefficients a_n resulting in $\xi_{100}\neq 0$ [see Eqs. (17), (19), (20), and (25)]. For $T>T_\lambda(\rho)$, only the trivial solution $M=0$ will be obtained at $H=0$.

5. Thermodynamic consistency

According to the thermodynamic relations $\mathcal{K}_T^{-1}=\rho(\partial P/\partial\rho)_{T,H}$ and $P=\rho/\beta-(\partial\mathcal{F}^*/\partial V)_{T,H}$, with $\mathcal{U}^*=(\partial\beta\mathcal{F}^*/\partial\beta)_{V,H}$, where $\mathcal{U}^*=\mathcal{U}-NHM$ and $\mathcal{F}^*$ denotes the excess Helmholtz free energy, there are two additional possibilities for the pressure evaluation apart from the virial equation. Integrating the above relations with respect to density and inverse temperature one obtains the pressure via the compressibility route

$$P_{\mathcal{K}}(\rho,T,H) = \int_0^\rho \frac{d\rho'}{\rho'\mathcal{K}_T(\rho',T,H)} \quad (34)$$

and energy route

$$P_{\mathcal{U}}(\rho,T,H) = \frac{\rho}{\beta} + \frac{\rho^2}{\beta}\int_0^\beta \left(\frac{\mathcal{U}^*(\rho,\beta',H)/N}{\partial\rho} \right)_{\beta',H} d\beta', \quad (35)$$

where $\mathcal{U}(\rho,T,H)/N$ and $\mathcal{K}_T(\rho,T,H)$ are defined according to Eqs. (22) and (23), respectively. Strictly speaking, the virial [Eq. (24)], compressibility [Eq. (34)], and energy [Eq. (35)] routes are completely equivalent and should lead to the same results, i.e., $P=P_{\mathcal{K}}=P_{\mathcal{U}}$, provided of course the one- and two-body correlation functions $\xi(\varphi), g(r,\varphi_1,\varphi_2)$ or $h(r,\varphi_1,\varphi_2), c(r,\varphi_1,\varphi_2)$ are calculated exactly. Integral equation theories yield only an approximate estimate of these

functions because of the approximate character of the bridge function $B(r,\varphi_1,\varphi_2)$, so that, in general, the quantities $P, P_{\mathcal{K}}$, and $P_{\mathcal{U}}$ will differ to some extent. For the same reason, the chemical potential obtained directly in terms of correlation functions [Eq. (A16)] will differ from its thermodynamic counterpart [Eq. (32)], i.e., $\mu^* \neq \mu_P^*$.

The thermodynamic self-consistency can be enforced by introducing corrections to the bridge function. For instance, in the self-consistent OZ approach (SCOZA), which in its original formulation was implemented only for simple isotropic hard-sphere Yukawa (HSY) systems [25,27,29], such corrections lead to a multiplication of the MSA direct correlation function $c(r)$ by some state dependent function $K(\rho,T)$ for $r>\sigma$. The SCOZA can be extended to our anisotropic soft-core *XY* fluid in the presence of an external field H by introducing a similar function $K(\rho,T,H)$ as a multiplier at the inverse temperature β in the SMSA closure [i.e., by formally replacing β by $\beta K(\rho,T,H)$ in Eqs. (6)–(8)]. Then $K(\rho,T,H)$ is determined by the requirement of thermodynamic consistency between the energy and compressibility routes, $P_{\mathcal{U}}(\rho,T,H)=P_{\mathcal{K}}(\rho,T,H)$. In a similar manner, the generalized MSA (GMSA) introduced originally for nonmagnetic HSY fluids [44], can be extended to a GSMSA (generalized soft MSA) level for our magnetic soft-core fluid by modifying the partitioning scheme. Then the long-ranged part of the potential [see equation just after Eq. (8)] is shifted by the quantity

$$\Delta u_1 = -[\Delta I(r) + \Delta J(r)\cos(\varphi_1-\varphi_2)]\exp[-\beta\phi(r)],$$

where $\Delta I(r)=\Delta J(r)/\mathcal{R}=\mathcal{E}\sigma\exp[-\mathcal{Z}(r-\sigma)]/r$. The three state-dependent functions $\mathcal{E}(\rho,T,H)$, $\mathcal{Z}(\rho,T,H)$, and $\mathcal{R}(\rho,T,H)$ can then be determined by the requirement of the full thermodynamic consistency, i.e., by satisfying the three conditions $P_{\mathcal{K}}=P$, $P_{\mathcal{U}}=P$, and $\mu_P=\mu$. In view of the anisotropy and softness, this leads to a significant sophistication of the calculations. For instance, the pressure evaluation via the compressibility [Eq. (34)] and energy [Eq. (35)] routes requires thermodynamic integration and differentiation over a wide range of temperature and density points, that can be performed only numerically and is very time consuming. They go beyond the scope of the present study and will be considered elsewhere. In this paper for the sake of simplicity, we will use the virial pressure [Eq. (24)] within the SMSA closure [Eqs. (6)–(8)] together with the Maxwell construction [Eq. (33)] when evaluating the phase coexistence densities [Eq. (31)] between gas and liquid states.

III. RESULTS

The coupled set of AOZ-SMSA-BGY and AOZ-SMSA-LMBW equations (6), (15), (19), or (20) was solved iteratively by adapting the MDIIS (modified direct inversion in the iterative subspace) algorithm originally proposed in Ref. [45] and developed in Ref. [8] when handling the Ising IE equations. At given values of ρ, T, and H, the iterations started from initial guesses for $c_{nml}(r)$ and a_n, and the Fourier-transformed functions $c_{nml}(k)$ were calculated. Then the total correlation function in k space was obtained by solving analytically the OZ equation (15) as $\mathbf{h}^{(l)}(k)=[\mathbf{I}-\rho\mathbf{c}^{(l)}(k)\boldsymbol{\xi}^{(l)}]^{-1}\mathbf{c}^{(l)}(k)$, where $\mathbf{h}^{(l)}$, $\mathbf{c}^{(l)}$, and $\boldsymbol{\xi}^{(l)}$ are the square matrices with the elements h_{nml}, c_{nml}, and ξ_{nml}, respectively, for each fixed $l=0$ or 1, and $\mathbf{I}$ denotes the unit matrix. Applying the backward Fourier transform yields $\mathbf{h}(r)=[1/(2\pi)^3]\int\mathbf{h}(k)\sin(kr)/(kr)d\mathbf{k}$. With the current values of $\mathbf{c}(r)$, $\mathbf{h}(r)$, and a_n, the residuals to the closure relation [Eq. (6)] and BGY [Eq. (19)] or LMBW [Eq. (20)] equations are evaluated. Using them, the new values of $\mathbf{c}(r)$ and a_n are updated according to the MDIIS corrections, and the iteration procedure is repeated until the solutions converge to within a relative root mean square residual accuracy of 10^{-6}. The integration in Eqs. (14), (16), and (18) with respect to angle variables was carried out by Gauss-Chebyshev quadratures with the number of knots varying from $\mathcal{M}=8$ to 32 with growing H from 0 to $1000\epsilon_J$. The number of harmonics involved was $\mathcal{N}=3$. Further increase of $\mathcal{M}$ and $\mathcal{N}$ does not affect the solutions.

The ratio R of the strengths of magnetic to nonmagnetic interactions was defined as $R=\epsilon_J/\epsilon_l$. The strength ε of the SC potential [Eq. (3)] was set to ϵ_J. This corresponds to a moderate softness of φ with respect to the total potential [see Eqs. (1) and (7)]. Note that in the limit $\varepsilon\to\infty$, the potential φ will tend to the HS function [Eq. (4)] with the hard sphere diameter $\sqrt[6]{2}\sigma$. The dimensionless quantities $\rho^*=\rho\sigma^3$, $T^*=k_BT/\epsilon_J$, $H^*=H/\epsilon_J$, and $z_{1,2}^*=z_{1,2}\sigma$ were chosen in the presentation of the results.

The simulations were carried out using the Gibbs ensemble MC (GEMC) method [47] and the grand canonical ensemble MC approach combined with multiple-histogram-reweighting (MHR) techniques [48] for evaluating the gas-liquid and liquid-liquid coexistences, while the Binder crossing scheme [21,49] based on canonical MC simulations was utilized to determine the paramagnetic-ferromagnetic transition (at $H=0$). Other simulation details are similar to those reported in Refs. [7,8,21].

A. The ideal system ($R=\infty$)

In Fig. 1 we compare the AOZ-SMSA-BGY and AOZ-SMSA-LMBW phase diagrams obtained for the ideal ($R=\infty$) *XY* fluid with $z_1^*=1$ at various external fields H with the corresponding GEMC and MHR simulation data. As can be seen, at $H=0$, a tricritical point separates the second-order paramagnetic-ferromagnetic phase transition line from the first-order transition between a paramagnetic gas and a ferromagnetic liquid. On turning on the external field, the tricritical point disappears and transforms into a critical one related to the transition between gas and liquid states. The H dependence of the gas-liquid critical temperature and density is nonmonotonic (see also Fig. 3 below). This is contrary to the Ising spin fluids [8], where the nonmonotonicity arises only in the nonideal regime.

Samples of the corresponding SCMF [7] binodals are included in Fig. 1 as well to demonstrate the obvious advantage of the IE theory over the MF approximation. The SCMF binodals were obtained [for $I(r)=0$] on the basis of a soft-core version of the MF theory introduced recently by us in Ref. [7]. On the other hand, the AOZ-SMSA-BGY approach

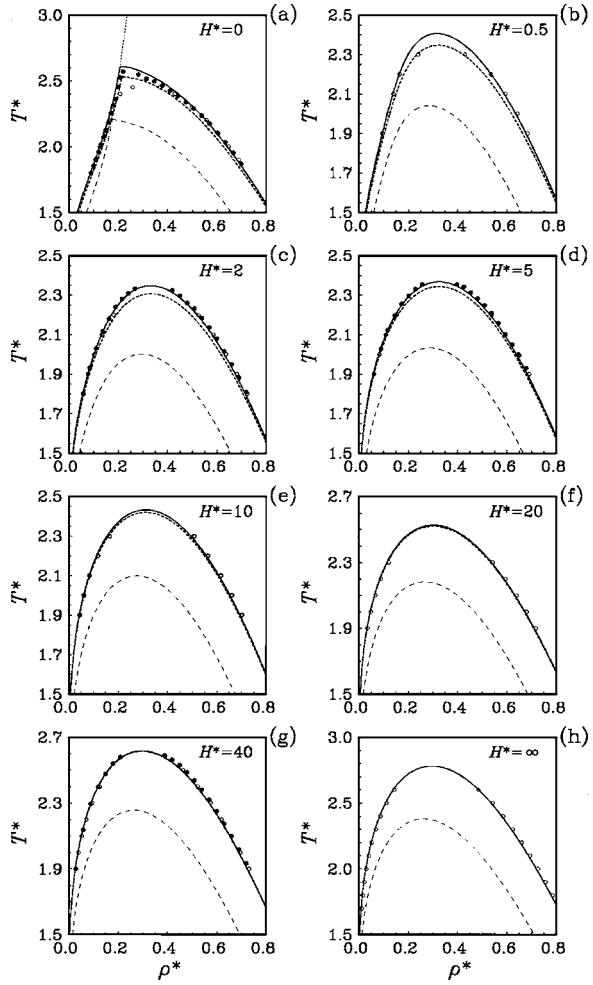

FIG. 1. The gas-liquid coexistence densities ρ^* as a function of temperature T^* obtained within the AOZ-SMSA-BGY integral equation approach (bold curves) for the ideal ($R=\infty$) soft-core *XY*-spin fluid with $z_1^*=1$ and different values of the external field, $H^*=0$, 0.5, 2, 5, 10, 20, 40, and ∞. The AOZ-SMSA-LMBW and SCMF results are plotted correspondingly by bold short- and thin long-dashed curves. The GEMC and MHR simulation data are shown as open and full circles, respectively. The paramagnetic-ferromagnetic phase transition [at $H^*=0$, subset (a)] is presented by the dotted curve.

leads to more accurate predictions of the gas-liquid coexistence densities with respect to the AOZ-SMSA-LMBW scheme. The latter scheme thus appears to be more sensitive to slight uncertainties in the two-body correlation functions g and c [see Eqs. (9) and (10)] introduced by the approximate SMSA bridge function [Eq. (8)]. With increasing H the influence of these uncertainties vanishes because then the main contribution to the one-body function ξ will be due to the interactions of spins with the external field, rather than the internal interactions between themselves. For this reason, the differences between the AOZ-SMSA-BGY and AOZ-SMSA-LMBW results decrease with rising external field and disappear completely in the limit $H\to\infty$. Note also that contrary to the theoretical binodals, the GEMC and MHR coexistence curves terminate when approaching the critical regions. This is because of the appearance of huge density fluctuations

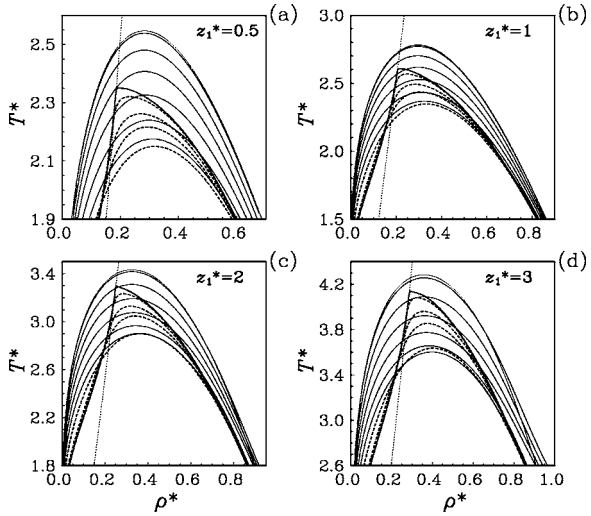

FIG. 2. The liquid-gas coexistence densities as a function of temperature obtained within the AOZ-SMSA-BGY integral equation approach for the soft-core ideal *XY*-spin fluid at different values, $z_1^*=0.5$, 1, 2, and 3, of the inverse screening length [subsets (a), (b), (c), and (d), respectively] as well as different values of the external field, namely, top to bottom (the set of dashed curves), $H^*=0.01$, 0.1, 0.3, and 2, as well as, bottom to top (the set of solid curves), $H^*=5$, 10, 20, 40, 100, 1000, and ∞ (within each subset). The bold curves correspond to the case $H=0$. The paramagnetic-ferromagnetic phase transition (at $H^*=0$) is plotted by the dotted lines.

which cannot be properly handled within finite simulation boxes. Nevertheless, the MHR technique allows to approach critical points more closely and should be considered as preferable to the GEMC method. In view of the above, all other results will be performed within the more precise AOZ-SMSA-BGY theory and MHR simulation technique (not involving the AOZ-SMSA-LMBW and GEMC schemes).

The influence of changing the screening radius of magnetic interactions on the AOZ-SMSA-BGY phase diagram is demonstrated in Fig. 2. As was mentioned in Sec. II A, the HSMF results will not depend on the screening radius by definition, while within the SCMF theory [7] a slight dependence on z_1 should arise due to the softness of the nonmagnetic repulsion potential. Using the more precise AOZ-SMSA-BGY integral equation approach, one observes an obvious z dependence of the coexistence densities for all values of the external field. The topology of the phase diagram remains, however, the same and is not affected by varying the screening radius. As in the case of the ideal Ising fluid [8], the IE approach predicts a tricritical point behavior for the ideal *XY* fluid at $H=0$ for any z (and not a critical end point in addition to a gas-liquid critical one, as was suggested for the ideal Heisenberg fluid [13]).

The dependencies of the gas-liquid critical temperature T_c and critical density ρ_c on the external field H are plotted in detail in subsets (a) and (b) of Fig. 3, respectively. As can be seen, varying z_1 (this quantity will be denoted below simply as z) does not change the tendency of functions $T_c(H)$ and $\rho_c(H)$ to behave nonmonotonically. At small inverse screening radii ($z^*<0.5$), the AOZ-SMSA-BGY and SCMF results

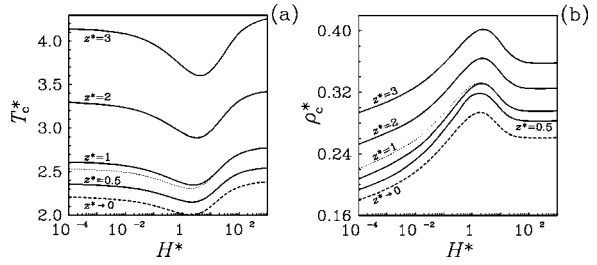

FIG. 3. The critical temperature T_c^* [subset (a)] and critical density ρ_c^* [subset (b)] as functions of the external field H^*, evaluated within the AOZ-SMSA-BGY approach for the soft-core ideal *XY*-spin fluid at various values of the inverse screening length z^*. The AOZ-SMSA-LMBW function is plotted for $z^*=1$ by the dotted curves. At $z^*\to 0$, the result corresponds to the SCMF theory (dashed curves).

are very close to one another. The reason is that in the Kac limit $z\to 0$, the SCMF theory should lead to exact results provided the equation of state for the reference (nonmagnetic soft-core fluid) system is exact too. Indeed, at $z\to 0$ the magnitude $2(z\sigma)^2/(z\sigma+1)$ of the magnetic potential vanishes, whereas the screening length $1/z$ tends to infinity. Under such conditions, the magnetic interactions can be treated as an infinitesimally small perturbation of the reference potential, making the assumptions of the MF theory exact.

The paramagnetic-ferromagnetic phase transition (which takes place only at $H^*=0$) obtained within the AOZ-SMSA-BGY approach is shown in Fig. 4(a) for the set $z^*=0.5$, 1, 2, 3, and 5 of inverse screening radius over a wide temperature and density region. We see that the dependence of the Curie temperature T_λ on ρ is nonlinear contrary to the HSMF prediction, where the function $T_\lambda^*=4\pi\rho^*$ increases linearly with rising ρ independently of z. Within the accurate AOZ-SMSA-BGY approach, the linear dependence of T_λ on ρ is recovered only in the Kac limit $z\to 0$. At moderate and large values of z, namely, at $z^*\geqslant 2$, the deviations from the limiting behavior are considerable. At smaller inverse screening radii $z^*<2$, both AOZ-SMSA-BGY and SCMF theories agree quite well. This is illustrated in Fig. 4(b) for the particular case $z^*=1$, where the theoretical results are practically indistinguishable from the MC simulation data.

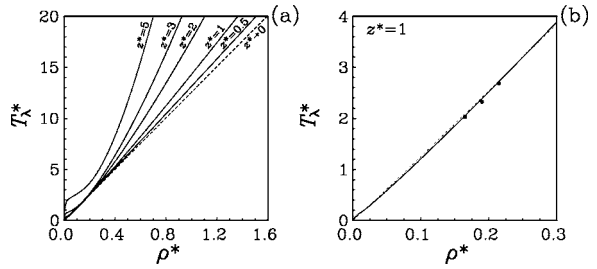

FIG. 4. (a) The paramagnetic-ferromagnetic transition temperature T_λ^* obtained at $H^*=0$ within the AOZ-SMSA-BGY integral equation approach for the soft-core ideal *XY*-spin fluid for different values of inverse screening length, from right to left, $z^*=0.5$, 1, 2, 3, and 5. The result of the standard HSMF theory is plotted as the dashed straight line and relates to the case $z^*\to 0$. (b) The results of the SCMF and AOZ-SMSA-BGY theories for the case $z^*=1$ are shown as dashed and solid curves, respectively, in comparison with canonical MC simulation data (circles).

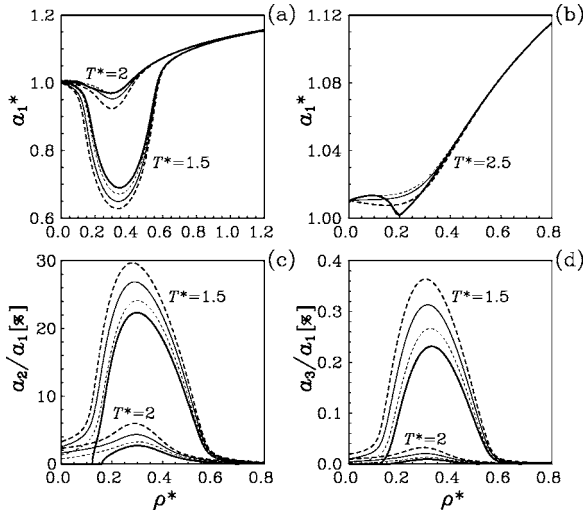

FIG. 5. The ratio of the first-harmonic coefficient in the expansion of the one-particle distribution function evaluated within the AOZ-SMSA-BGY approach for the ideal *XY*-spin fluid model ($z_1^*=1$) to the effective magnetic field obtained by the MF theory [subsets (a) and (b)]. The influence of the second- and third-harmonic coefficients is shown in subsets (c) and (d), respectively. The results are plotted versus density at several temperatures and external field values by the bold solid, short-dashed, thin solid, and long-dashed curves for the cases $H^*=0$, 2, 5, and 10, respectively.

In order to ensure that the number of harmonics $\mathcal{N}=3$ chosen is indeed enough for precise AOZ-SMSA-BGY calculations, we explicitly considered the contributions of the expansion coefficients a_1, a_2, and a_3 to the one-body distribution function $\xi(\varphi)$ [see Eq. (17)]. For $\mathcal{N}=3$, this function can be cast in the form

$$\xi(\varphi)\approx\frac{1}{Z}\exp\{\beta[(H+a_1)\cos\varphi+a_2\cos 2\varphi+a_3\cos 3\varphi]\},$$

where higher-order harmonics have been neglected. The MF theory corresponds, in fact, to the case $\mathcal{N}=1$ with $a_1^{\mathrm{MF}}=a\rho M=h_{\mathrm{MF}}$ and $a_2^{\mathrm{MF}}=a_3^{\mathrm{MF}}=0$, where $a=8\pi\epsilon_J\sigma^3$ and h_{MF} is the effective internal magnetic field caused by spin-spin interactions [7]. Then the function $\xi(\varphi)$ simply reduces to that corresponding to a noninteracting spin fluid in the presence of the effective external field $H_{\mathrm{eff}}^{\mathrm{MF}}=H+h_{\mathrm{MF}}$. The ratio $a_1^*=a_1/a_1^{\mathrm{MF}}$ of first-harmonic coefficients evaluated within the AOZ-SMSA-BGY and MF theories is plotted in Fig. 5 in a wide density region at some characteristic values of temperature and external field.

As can be seen, the deviations of a_1^* from unity are significant, especially at moderate densities and low temperatures, and may exceed 35%. The MF theory overestimates the genuine internal magnetic field at moderate ρ and low T, where $a_1^*<1$, and underestimates it for large densities and high temperatures, where $a_1^*>1$. Only in the low density limit $\rho\to 0$, where $a_1^*\to 1$, do the AOZ-SMSA-BGY and MF results tend to one another. On the other hand, the influence of the second-harmonic coefficient a_2 can also be significant

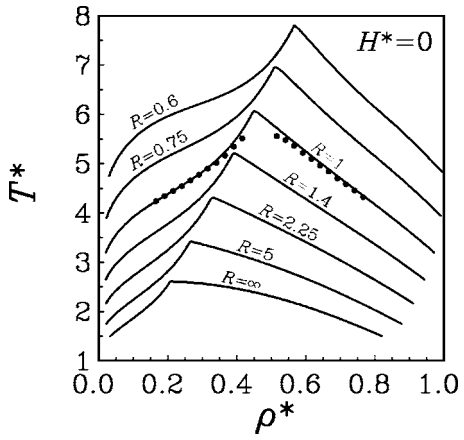

FIG. 6. The gas-liquid coexistence densities as a function of temperature obtained within the AOZ-SMSA-BGY approach for the soft-core nonideal *XY*-spin fluid with $z_1^*=z_2^*=1$ at $H^*=0$ for large values of R. The MHR simulation data for $R=1$ are shown as circles.

and achieve of order 30% in magnitude with respect to a_1 [see Fig. 5(b)]. Therefore, the one-body function cannot be reduced, in general, to a simple noninteracting representation for any value of $H_{\mathrm{eff}}=H+a_1$. Only beginning from the third-harmonic coefficient a_3, does the unharmonicity become very small (less than 1%), so that the influence of the higher-order terms a_n with $n>\mathcal{N}=3$ can be neglected completely. Similar behavior is observed with two-body expansion coefficients h_{nml}, g_{nml} and c_{nml} which vanish for $n,m>\mathcal{N}$.

B. Nonideal models ($0<R<\infty$)

1. Zero magnetic field

The AOZ-SMSA-BGY phase diagrams of the nonideal *XY* fluid at $H=0$ are plotted in Figs. 6 and 7 for different ratios R of strengths of magnetic to nonmagnetic interactions with $z_1^*=z_2^*=1$. The MHR results are also included for some values of R in order to show that the approach proposed is able to describe quantitatively the phase behavior not only in the ideal case but also in the presence of nonmagnetic attraction interactions. As can be seen in Fig. 6, when the ratio

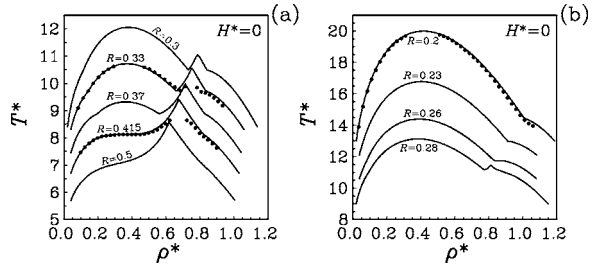

FIG. 7. The gas-liquid and liquid-liquid coexistence densities as a function of temperature obtained within the AOZ-SMSA-BGY approach for the soft-core nonideal *XY*-spin fluid with $z_1^*=z_2^*=1$ at $H=0$ for moderate [subset (a)] and small [subset (b)] values of R. The MHR simulation data for $R=0.415$, 0.33, and 0.2 are shown as circles.

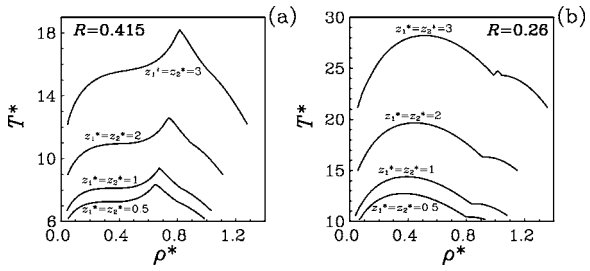

FIG. 8. The coexistence densities as a function of temperature T^* obtained within the AOZ-SMSA-BGY approach for the nonideal *XY* spin fluid at $R=0.415$ [subset (a)] and $R=0.26$ [subset (b)] corresponding to different values $z_1^*=z_2^*=0.5$, 1, 2, and 3, of the inverse screening radius.

$0.415\leqslant R\leqslant\infty$ is relatively large, the nonideal system exhibits a tricritical point behavior, similarly to the ideal case $R=\infty$.

With decreasing R, the shape of the phase coexistence curves changes considerably (see Fig. 7). At moderate ratios $0.26=R_{\mathrm{l}}<R<R_{\mathrm{u}}=0.415$ (where R_{u} and R_{l} are the upper and lower boundary values, respectively), we have two first-order transitions, namely, between a paramagnetic gas and a paramagnetic liquid as well as between a paramagnetic liquid and a ferromagnetic liquid (instead of only one first-order transition between a paramagnetic gas and a ferromagnetic liquid as in the above ideal-like case $0.415\leqslant R\leqslant\infty$). They are complemented by the presence of the tricritical and critical points, respectively. Here, a triple point occurs too. In this point, a rarefied paramagnetic gas, a moderately dense paramagnetic liquid, and a highly dense ferromagnetic liquid all coexist at the same temperature T and pressure P. The sophistication of the phase diagram behavior with decreasing R is explained by an increased weight of nonmagnetic attractions in the system and their subtle interplay with spin interactions. For small $0<R\leqslant 0.26$, the nonmagnetic interactions become too strong. As a result, the tricritical point disappears and transforms into a critical end point. At the same time, the gas-liquid critical point remains and shifts away from the critical end point with further decreasing R.

Changing the screening radii z_1 and z_2 can also result in qualitative modification of the phase diagram topology as is demonstrated in Figs. 8 and 9. In the case $z_1=z_2=z$ it can be concluded that the upper boundary value $R_{\mathrm{u}}(z)$ (which is equal to 0.415 at $z^*=1$) and the lower boundary value $R_{\mathrm{l}}(z)$ (taking the value 0.26 at $z^*=1$) both decrease with increasing $z=z_1=z_2$. A more complicated behavior can be observed when $z_1\neq z_2$. Here, the boundaries R_{u} and R_{l} should be considered as functions of two variables z_1 and z_2. It can be seen that these functions are not monotonic. In particular, the functions $R_{\mathrm{u}}(z_1,z_2)$ and $R_{\mathrm{l}}(z_1,z_2)$ increase with increasing z_2 at constant $z_1^*=1$, but decrease with rising z_1^* at fixed $z_2^*=1$.

The AOZ-SMSA-BGY predictions on the paramagnetic-ferromagnetic transition in the nonideal *XY* fluid at $H=0$ are shown in Fig. 10 for various values of R in a wide region of the temperature-density plane. Samples of canonical MC simulation data are also included. As was established in the case of the ideal fluid ($R=\infty$), the Curie temperature T_λ^* depends considerably on the screening radius z [see Fig. 4(a)].

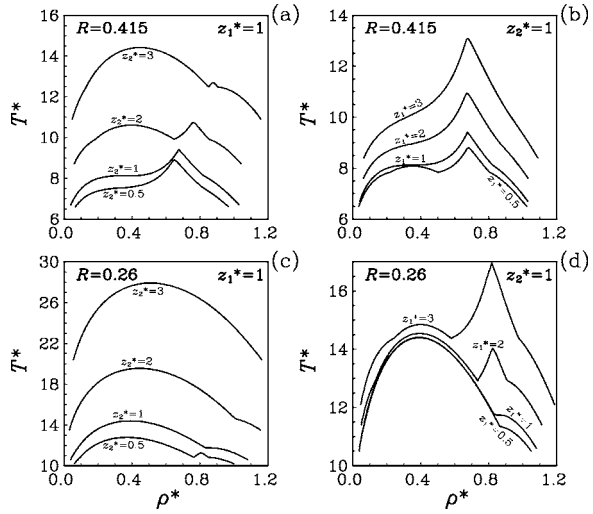

FIG. 9. The same as in Fig. 8 but for $z_1 \neq z_2$ at $R=0.415$ [subsets (a) and (b)] and $R=0.26$ [subsets (c) and (d)].

Our calculations show that the function $T_\lambda(\rho)$ may also exhibit a significant dependence on the parameter R, especially at low densities (see Fig. 10). This is contrary to predictions of the HSMF and SCMF theories which lead to values of $T_\lambda^*(\rho^*)$ independent of R. For large densities ($\rho^*>1$), all the AOZ-SMSA-BGY curves begin to converge to the same function and the R dependence vanishes. The latter function is almost linear in density, however, it does not coincide with the HSMF and SCMF Curie lines.

2. Nonzero magnetic field

The complete AOZ-SMSA-BGY phase diagrams of the nonideal *XY* fluid in the presence of the external field are plotted in Fig. 11 for various values of R and H. For the purpose of comparison, the samples of the MHR simulation data are also shown in this figure [see subset (e)] for a value of $R=0.37$ and a set of different H. In view of the results presented in Figs. 6, 7, and 11, we can identify four types of phase diagram topology overall. For large values $R \geqslant 0.415$ (type I), the system exhibits an ideal-like behavior with the presence of a tricritical point at $H=0$ and gas-liquid critical points for $H \neq 0$ at each R. At moderate ratios $0.26 < R < 0.415$ (type II), the gas-liquid critical point exists simultaneously with the tricritical and triple ones at $H=0$. For $H \neq 0$, the tricritical point transforms into a critical one which relates to the transition between a moderately magnetized liquid and a strongly magnetized liquid. The triple points can exist at $H \neq 0$ as well and describe then the simultaneous

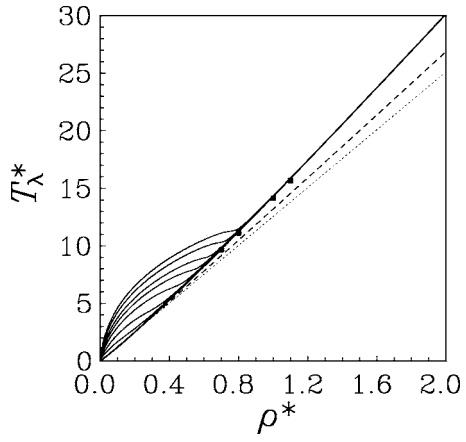

FIG. 10. The paramagnetic-ferromagnetic Curie curves evaluated at $H=0$ using the AOZ-SMSA-BGY theory for the soft-core nonideal *XY*-spin fluid with $z_1^*=z_2^*=1$ at different values of the system parameter, top to bottom, $R=0.2$, 0.23, 0.28, 0.33, 0.415, 0.6, 1, and ∞. The results of the HSMF and SCMF approaches are plotted as the dotted and dashed curves, respectively. The canonical MC simulation points are shown by circles ($R=0.33$) and squares ($R=0.2$).

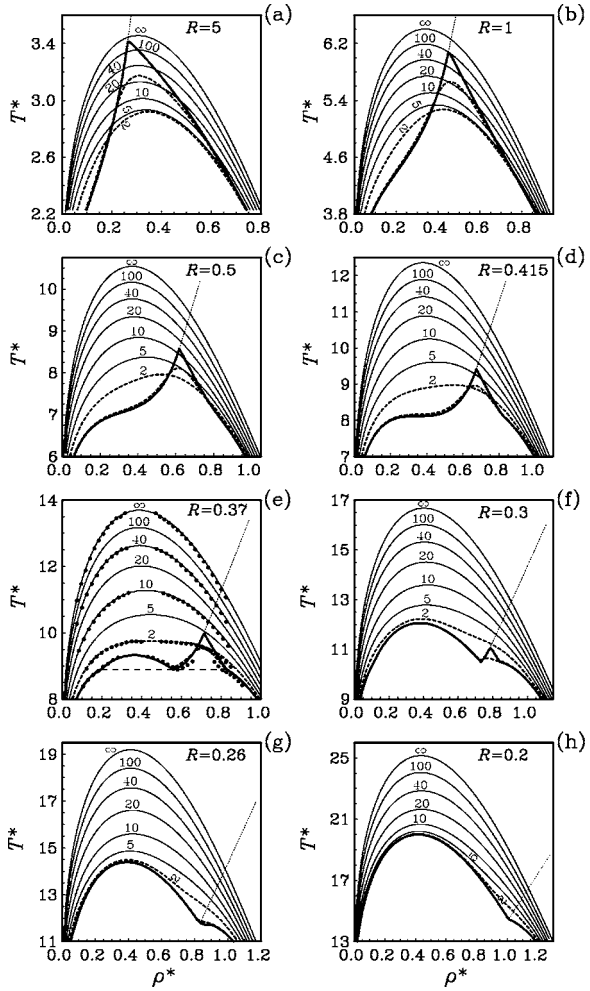

FIG. 11. The complete thermodynamic phase diagrams obtained for the soft-core nonideal *XY*-spin fluid with $z_1^*=z_2^*=1$ using the AOZ-SMSA-BGY approach at some typical values of $R=5$, 1, 0.5, 0.415, 0.37, 0.3, 0.26, and 0.2 [subsets (a), (b), (c), (d), (e), (f), (g), and (h), respectively]. The families of the coexistence curves in each of the subsets correspond to different values of the external field, namely, top to bottom (the set of dashed curves), $H^*=0.1$ and 2, as well as, bottom to top (the set of solid curves), $H^*=5$, 10, 20, 40, 100, and ∞. The bold curves relate to the case $H=0$. The MHR simulation data for $R=0.37$ and $H^*=0$, 2, 10, 40, and ∞ are shown in subset (e) as circles. The paramagnetic-ferromagnetic phase transition (at $H^*=0$) is plotted by the dotted curves.

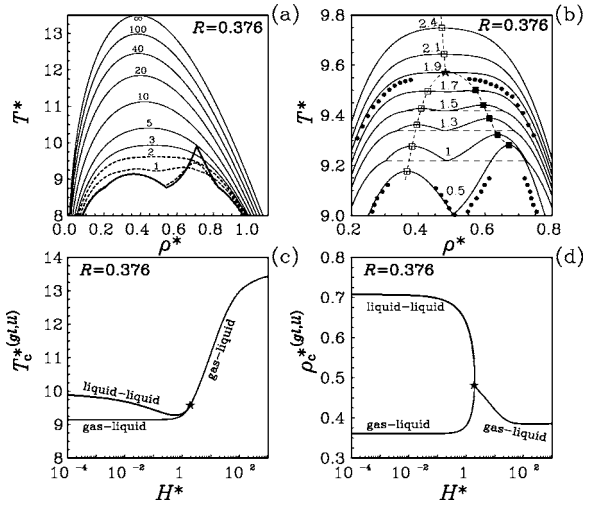

FIG. 12. The thermodynamic phase diagrams obtained within the AOZ-SMSA-BGY approach for the soft-core nonideal *XY*-spin fluid with $z_1^*=z_2^*=1$ at $R=R_{vL}=0.376$ and $H^*=0$, 0.1, 1, 2, 3, 5, 10, 20, 40, 100, and ∞ [subset (a)]. A more detailed phase behavior near the asymmetric tricritical point is presented in subset (b) for (bottom to top) $H^*=0.5$, 1, 1.3, 1.5, 1.7, 1.9, 2.1, and 2.4. Samples of the MHR simulation data are presented in subset (b) for $H^*=0.5$ and 1.9 by circles. The gas-liquid (on the left) and liquid-liquid (on the right) critical points are shown as open and full squares, respectively, connected by dashed curves. The curves meet in the tricritical point (star). The triple points are represented by the horizontal dashed lines. The critical temperature and critical density of the gas-liquid and liquid-liquid phase transitions are plotted as functions of H^* in subsets (c) and (d), respectively.

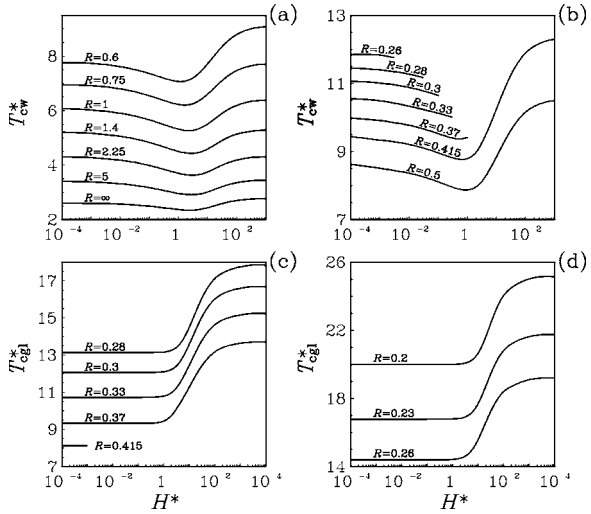

FIG. 13. The critical temperature of the wing lines T_{cw}^*, subsets (a) and (b), and the gas-liquid critical lines T_{cgl}^*, subsets (c) and (d), as a function of the external magnetic field H^* for the nonideal *XY*-spin fluid at different values of parameter R.

coexistence of three phases, namely, a weakly magnetized gas, a moderately magnetized liquid, and a strongly magnetized liquid. With increasing H, either the gas-liquid ($0.376<R<0.415$, type IIa) or liquid-liquid ($0.26<R<0.376$, type IIb) transition disappears in a critical end point at some finite $H(R)$. For larger values of H, only a gas-liquid transition is present, so that the gas-liquid critical point extends to infinite field in any case.

For small $0<R\leqslant 0.26$ (type III), the translational interaction dominates over the spin one, leaving only the gas-liquid transition, whereas the tricritical point at $H=0$ transforms into a critical end point. For $H\to\infty$, the system at any R behaves like a simple nonmagnetic fluid with the interparticle potential $u(r)=\phi(r)-I(r)-J(r)$. Then all spins align exactly along the field vector $\mathbf{H}$, so that $\cos(\varphi_1-\varphi_2)=1$ for any pair of particles [see Eq. (7)].

In the special case $R=R_{vL}=0.376$, the gas-liquid and liquid-liquid critical lines merge into one point at some finite value of the external field. It is an asymmetric tricritical point which is also known as a van Laar point [50] in the global phase diagram. The van Laar-like behavior is presented in Fig. 12 using $(\rho,T),(H,T)$, and (H,ρ) projections. The computations show that such a specific tricritical point is identified at $H_{vL}^*\approx 1.9$ with $\rho_{vL}^*\approx 0.48$ and $T_{vL}^*\approx 9.6$.

The gas-liquid critical temperature T_{cgl}^*, the liquid-liquid (wing) critical temperature T_{cw}^*, as well as the corresponding densities ρ_{cgl}^* and ρ_{cw}^* are shown in detail as functions of the strength H^* of the external field in Figs. 13 and 14, respectively. We mention that both gas-liquid and liquid-liquid phase transitions may exist only in the region of type II, $0.26=R_l<R<R_u=0.415$, of the global phase diagram. For type I [subset (a)], the wing line will correspond to the gas-liquid critical point (no liquid-liquid phase transitions are present in R regions corresponding to types I and III). As can be seen, the function T_{cw}^* is nonmonotonic in H for $0.376=R_{vL}<R<\infty$, i.e., in the whole R interval where this function can exist for arbitrary fields $0\leqslant H^*\leqslant\infty$. The position of the minimum in $T_{cw}^*(H^*)$ shifts from $H^*\sim 3$ to 1 with decreasing R. For $R<R_{vL}$; the wing line terminates at some finite value $H_{cew}^*(R)$ [subset (b) of Fig. 13] until it disappears at all at $R<R_l=0.26$. The wing line density $\rho_{cw}^*(H^*)$ also exhibits a nonmonotonic field dependence in the interval $0.6\leqslant R<\infty$ with the presence of a maximum at $H^*(R)\sim 0.1$

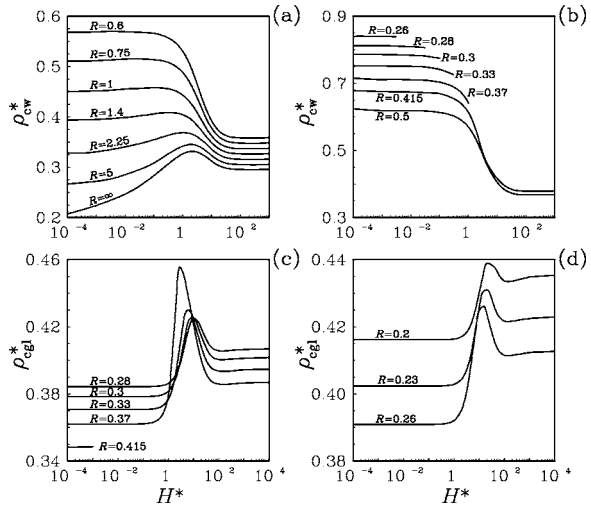

FIG. 14. The critical density of the wing lines ρ_{cw}^*, subsets (a) and (b), and the gas-liquid critical lines ρ_{cgl}^*, subsets (c) and (d), as a function of the external magnetic field H^* for the nonideal *XY*-spin fluid at different values of R.

to 2. For $R<0.6$, it decreases monotonically [see subset (b) of Fig. 14].

On the other hand, for $0.376=R_{vL}<R<R_u=0.415$ the gas-liquid critical line ends in a critical end point at some finite value $H^*_{cegl}(R)$ [subset (c) of Figs. 13 and 14]. For $R\leqslant R_{vL}$, the gas-liquid transition line exists for arbitrary fields $0\leqslant H^*\leqslant\infty$. The critical temperature $T^*_{cgl}(H^*)$ of this transition increases always monotonically with increasing H^* [subsets (c) and (d) of Fig. 13], whereas the critical density $\rho^*_{cgl}(H^*)$ is always a nonmonotonic function exhibiting a maximum at $H^*\sim 3$ to 30 depending on R [see subsets (c) and (d) of Fig. 14].

It is worth pointing out that phase behavior similar to that presented in Figs. 1–14 for the *XY*-spin fluid has been recently found by us within the IE approach for the Ising fluid model [8]. The phase diagram topologies found at $H=0$ for the *XY* and Ising fluids are also observed for other systems, such as symmetric binary nonmagnetic mixtures [24–31], mixtures of ^{3}He-^{4}He [22,34,35], the Heisenberg fluid [4,19] or the Stockmayer fluid [51]. The van Laar point has earlier been realized in symmetric mixtures [52] and Ising fluids [8]. We note also that all the types of the phase diagrams found in the present study for the *XY* fluid within the IE approach could be investigated within MF theory [4] as well. However, the disadvantage of the MF approach is that it can provide only a qualitative description. In particular, it produces boundary values R_u and R_l which are independent of z^*_1 and z^*_2. This corresponds, in fact, to the limiting behavior of the genuine functions $R_u(z_1,z_2)$ and $R_l(z_1,z_2)$ at $z^*_1=z^*_2\to 0$.

As can be seen from the results presented, the agreement between the AOZ-SMSA-BGY theory proposed and the simulations is quite satisfactory (see Figs. 1, 4, 6, 7, 11, and 12). Slight deviations appear only in the vicinity of critical points. This is explained by finite size effects in the simulations and the approximate character of the SMSA closure used in the theory. For the latter reason, the classical value $\beta=1/2$ of the critical exponent describing the gas-liquid binodal behavior $|\rho-\rho_c|\sim|T-T_c|^\beta$ near the critical point (ρ_c,T_c) is recovered (in particular, at $R=\infty$ and $H\neq 0$; see Fig. 1), instead of the value $\beta\approx 1/3$ known from the renormalization group analysis [53]. On the other hand, the crossover to the tricritical value $\beta=1/4$ can be observed near the van Laar point at $R=0.376$ and $H^*=1.9$ [Fig. 12(b)]. More precise IE calculations near critical points are possible provided the thermodynamic self-consistency is satisfied (see Sec. II C 5).

IV. CONCLUSION

In this paper, we have proposed a technique to investigate orientationally ordered fluids with planar spins. The technique combines the standard integral equation method with appropriate expansions of the anisotropic correlation functions in terms of orthogonal polynomials. This reduces the anisotropic integral equation calculations to those inherent in a homogeneous mixture of simple monatomic fluids and thus presents now no numerical difficulties. Detailed comparisons with GEMC and MHR simulations have shown that the proposed AOZ-SMSA-BGY approach is powerful enough to give a quantitative description of phase transitions in the *XY*-spin fluid systems.

The AOZ-SMSA-BGY method can also be extended to systems with dipole interactions in the presence of an external electric field. The present SMSA closure can be applied to Heisenberg spin and dipole fluids with soft-core repulsion potentials. These problems including the improvement of the thermodynamic self-consistency of the integral equation approach will be the subject of our future investigations.

ACKNOWLEDGMENTS

This work was supported in part by the Fonds zur Förderung der wissenschaftlichen Forschung under Project No. P15247. I.O. and I.M. thank the Fundamental Researches State Fund of the Ministry of Education and Science of Ukraine for support under Project No. 02.07/00303.

APPENDIX A: CHEMICAL POTENTIAL

The *XY*-spin fluid in an external magnetic field H is defined by the canonical partition function

$$\mathcal{Q}_N(V,T,H)=\frac{1}{N!\,\Lambda^{3N}}\int d\mathbf{q}^N\exp[-\beta U(\mathbf{r}^N,\varphi^N)], \tag{A1}$$

where $d\mathbf{q}^N=\Pi_{i=1}^N d\mathbf{r}_i d\varphi_i$ and U denotes the microscopic expression [see Eq. (1)] for the total potential energy of the system [the magnetization per particle, see Eq. (25), reduces to $M=(k_BT/N)\,\partial\ln\mathcal{Q}_N/\partial H$]. In classical statistical mechanics, the chemical potential can be directly connected with the partition function by the relation

$$\mu_\lambda=-k_BT\ln\left(\frac{\mathcal{Q}_{N+1}(\lambda)}{\mathcal{Q}_N}\right). \tag{A2}$$

It follows from the definition of the Helmholtz free energy $\mathcal{F}_N=-k_BT\ln\mathcal{Q}_N$ and thermodynamics relation $\mu=(\partial\mathcal{F}/\partial N)_{VTH}\equiv\mathcal{F}_{N+1}(\lambda)-\mathcal{F}_N$ in the limit $\lim_{N\to\infty}$. In our notation, the $(N+1)$th particle is considered as a separate (solute) body which couples to the (solvent) system by the parameter λ. In other words, the solute body interacts with all the other N solvent particles via the potential $u_\lambda(r,\varphi_1,\varphi_2)$, while the interaction $u(r,\varphi_1,\varphi_2)$ between solvent particles remains unchanged and independent of λ. Then

$$\mathcal{Q}_{N+1}(\lambda)=\frac{1}{(N+1)!\,\Lambda^{3(N+1)}}\int d\mathbf{q}^{N+1}\exp[-\beta(U+\Delta U_\lambda)] \tag{A3}$$

with $\Delta U_\lambda=H\cos(\varphi_{N+1})+\Sigma_{i=1}^N u_\lambda(|\mathbf{r}_i-\mathbf{r}_{N+1}|,\varphi_i,\varphi_{N+1})$. Differentiating Eq. (A2) with respect to λ in view of Eq. (A3) yields

$$\frac{\partial \mu_\lambda}{\partial \lambda} = \left\langle \frac{\partial \Delta U_\lambda(\mathbf{r}^{N+1}, \varphi^{N+1})}{\partial \lambda} \right\rangle_\lambda = \frac{\rho}{(2\pi)^2} \int d\mathbf{r}\, d\varphi_1 d\varphi_2 \times \xi(\varphi_1)\xi_\lambda(\varphi_2) g_\lambda(r, \varphi_1, \varphi_2) \frac{\partial u_\lambda(r, \varphi_1, \varphi_2)}{\partial \lambda}, \quad \text{(A4)}$$

where $\langle \cdots \rangle_\lambda = \int \cdots d\mathbf{q}^{N+1} \exp[-\beta(U+\Delta U_\lambda)]/[(N+1)!\Lambda^{3(N+1)}\mathcal{Q}_{N+1}(\lambda)]$ denotes the statistical averaging. Taking into account the equality $\mu \equiv \mu_{\lambda=1} = \mu_{\lambda=0} + \int_0^1 d\lambda\ \partial\mu_\lambda/\partial\lambda$, where $\mu_{\lambda=0} = -k_B T \ln \mathcal{Q}_{N+1}(\lambda=0)/\mathcal{Q}_N = k_B T[\ln(\rho\Lambda^3) - \ln Z_0]$, one immediately reproduces Eq. (30).

In order to find an explicit form of the λ dependence for functions $g_\lambda(r, \varphi_1, \varphi_2) = h_\lambda(r, \varphi_1, \varphi_2) + 1$ and $\xi_\lambda(\varphi_2)$, it is convenient to treat the solute and solvent subsystems as a binary mixture at infinite solute dilution. Then the solute-solvent total correlation function h_λ and the solute one-body distribution function ξ_λ can be found from the corresponding mixture AOZ and LMBW equations,

$$h_\lambda(r, \varphi_1, \varphi_2) = c_\lambda(r, \varphi_1, \varphi_2) + \frac{\rho}{2\pi} \int d\mathbf{r}'\, d\varphi \xi(\varphi) \times c(|\mathbf{r} - \mathbf{r}'|, \varphi_1, \varphi) h_\lambda(r', \varphi, \varphi_2) \quad \text{(A5)}$$

and

$$\frac{d}{d\varphi} \ln \frac{\xi_\lambda(\varphi)}{\xi_0(\varphi)} = \frac{\rho}{2\pi} \int d\mathbf{r}\, d\varphi' c_\lambda(r, \varphi, \varphi') \frac{d\xi(\varphi')}{d\varphi'}, \quad \text{(A6)}$$

respectively [they differ from the basic equations; see Eqs. (5) and (10)], complemented by the solute-solvent closure [see Eq. (6)]

$$g_\lambda(r, \varphi_1, \varphi_2) = \exp[-\beta u_\lambda(r, \varphi_1, \varphi_2) + h_\lambda(r, \varphi_1, \varphi_2) - c_\lambda(r, \varphi_1, \varphi_2) + B_\lambda(r, \varphi_1, \varphi_2)], \quad \text{(A7)}$$

where $c_\lambda(r, \varphi_1, \varphi_2)$ and $c(r, \varphi_1, \varphi_2)$ are the solute-solvent and solvent-solvent direct correlation functions, respectively, and $\xi(\varphi)$ is the solvent one-body distribution function. Taking the partial derivative $\partial u_\lambda(r, \varphi_1, \varphi_2)/\partial\lambda$ from the differentiation of Eq. (A7) with respect to λ, one finds

$$g_\lambda \frac{\partial u_\lambda}{\partial \lambda} = \frac{\partial}{\partial \lambda}\left(\frac{h_\lambda^2}{2} - c_\lambda + B_\lambda \right) - h_\lambda \frac{\partial c_\lambda}{\partial \lambda} + h_\lambda \frac{\partial B_\lambda}{\partial \lambda}. \quad \text{(A8)}$$

Despite a relative simple structure of Eq. (A8), we will come to significant difficulties when trying to perform the λ integration according to Eqs. (30) and (A4), because of the existence of the multiplier $\xi_\lambda(\varphi_2)$ which depends on λ in a complicated way [Eq. (A6)].

To avoid this, let us consider the solute insertion as a process during which the solute one-body distribution function $\xi_\lambda(\varphi)$ is constrained to be fixed (independent of λ) and equal to the one-body distribution function $\xi(\varphi)$ of the (solvent) system. The constraint $\xi_\lambda(\varphi) = \xi(\varphi)$ can be enforced by introducing an auxiliary external potential $v_\lambda(\varphi)$ which relates exclusively to the solute particle and vanishes when this particle is fully coupled to the system, i.e., $v_{\lambda=1}(\varphi) = 0$. Adding the corresponding external field term $-d\beta v_\lambda(\varphi)/d\varphi$ to the right-hand side of Eq. (A6) we obtain

$$\beta \frac{dv_\lambda(\varphi)}{d\varphi} = \frac{\rho}{2\pi} \int d\mathbf{r}\, d\varphi' c_\lambda(r, \varphi, \varphi') \frac{d\xi(\varphi')}{d\varphi'} - \frac{d}{d\varphi} \ln \zeta(\varphi), \quad \text{(A9)}$$

where $\zeta(\varphi) = \xi(\varphi)/\xi_0(\varphi)$ denotes the normalized one-body orientational distribution. The partition function then transforms to

$$\mathcal{Q}_{N+1}(\lambda) = \frac{1}{(N+1)\Lambda^{3(N+1)}} \int d\mathbf{q}^{N+1} \times \exp\{-\beta[U + \Delta U_\lambda + v_\lambda(\varphi_{N+1})]\}, \quad \text{(A10)}$$

so that now

$$\frac{\partial \mu_\lambda}{\partial \lambda} = \left\langle \frac{\partial v_\lambda}{\partial \lambda} \right\rangle_{\lambda, v_\lambda} + \left\langle \frac{\partial \Delta U_\lambda(\mathbf{r}^{N+1}, \varphi^{N+1})}{\partial \lambda} \right\rangle_{\lambda, v_\lambda}$$

and $\mu_{\lambda=0} = -k_B T \ln \mathcal{Q}_{N+1}(\lambda=0)/\mathcal{Q}_N = k_B T[\ln(\rho\Lambda^3) - \ln Z]$. Thus, Eq. (30) can be rewritten in the equivalent form

$$\mu^* = -k_B T \ln Z + w + \frac{\rho}{(2\pi)^2} \int_0^1 d\lambda \int d\mathbf{r}\, d\varphi_1 d\varphi_2 \times \xi(\varphi_1)\xi(\varphi_2) g_\lambda(r, \varphi_1, \varphi_2) \frac{\partial u_\lambda(r, \varphi_1, \varphi_2)}{\partial \lambda}, \quad \text{(A11)}$$

where $w = (1/2\pi)\int_0^1 d\lambda \int d\varphi\ \xi(\varphi)\, \partial v_\lambda(\varphi)/\partial\lambda$ denotes the additional work of turning on and varying the auxiliary external field.

The λ integration in the right-hand side of Eq. (A11) can already be performed readily. Indeed, substituting now the partial derivative $g_\lambda \partial u_\lambda/\partial\lambda$ from Eq. (A8) leads to the exact integration of the first term as $\int_0^1 d\lambda\ \partial[h_\lambda^2/2 - c_\lambda + B_\lambda]/\partial\lambda = h^2/2 - c + B$. The second term $h_\lambda \partial c_\lambda/\partial\lambda$ can also be reduced to an exact differential and thus integrated exactly. Using Eq. (A5) and the symmetry property $c(|\mathbf{r} - \mathbf{r}'|, \varphi_1, \varphi_2) = c(|\mathbf{r}' - \mathbf{r}|, \varphi_2, \varphi_1)$, it can be shown that

$$\int d\mathbf{r}\, d\varphi_1 d\varphi_2 \xi(\varphi_1)\xi(\varphi_2) h_\lambda(r, \varphi_1, \varphi_2) \frac{\partial c_\lambda(r, \varphi_1, \varphi_2)}{\partial \lambda} = \frac{1}{2}\frac{\partial}{\partial \lambda} \int d\mathbf{r}\, d\varphi_1 d\varphi_2 \xi(\varphi_1)\xi(\varphi_2) h_\lambda(r, \varphi_1, \varphi_2) c_\lambda(r, \varphi_1, \varphi_2). \quad \text{(A12)}$$

For the third term in the right-hand side of Eq. (A8) we use that $h_\lambda \partial B_\lambda/\partial\lambda = \partial(h_\lambda B_\lambda)/\partial\lambda - B_\lambda \partial h_\lambda/\partial\lambda$, while for the second term in the right-hand side of Eq. (A11) we obtain in view of Eq. (A9) that $w = (1/2\pi)\int d\varphi\ \xi(\varphi) \ln \zeta(\varphi)$. Then after some algebra, the excess chemical potential can be cast in the following explicit form:

$$\beta\mu^* = -\ln Z + \frac{1}{2\pi} \int d\varphi\ \xi(\varphi) \ln \zeta(\varphi) + \frac{\rho}{(2\pi)^2} \int d\mathbf{r}\, d\varphi_1 d\varphi_2 \xi(\varphi_1)\xi(\varphi_2) \left(\frac{1}{2}[h^2(r, \varphi_1, \varphi_2) - h(r, \varphi_1, \varphi_2) c(r, \varphi_1, \varphi_2)] - c(r, \varphi_1, \varphi_2) + g(r, \varphi_1, \varphi_2) B(r, \varphi_1, \varphi_2) \right)$$

$$-\int_0^1 \frac{\partial h_\lambda(r,\varphi_1,\varphi_2)}{\partial\lambda} B_\lambda(r,\varphi_1,\varphi_2)d\lambda\Bigg). \tag{A13}$$

Equation (A13) is an exact result (no approximations have been made up to this moment).

The λ integration in the last term of the right-hand side of Eq. (A13) can be performed using one or another form of the bridge function. For instance, for the HNC closure $B\equiv 0$, and this term will be absent. In principle, the λ integration should be path independent, i.e., invariant with respect to the way of turning on the interaction $u_\lambda(r,\varphi_1,\varphi_2)$ from $u_{\lambda=0}=0$ to $u_{\lambda=1}=u(r,\varphi_1,\varphi_2)$, provided the bridge function B_λ is exact. In actual calculations we can deal only with an approximate form of $B_\lambda(r,\varphi_1,\varphi_2)$ for which the λ integration will be already, generally speaking, path dependent (the problem with the path dependence for isotropic systems has been recently considered in detail in Ref. [54]). For a wide class of modern closures, the bridge function is believed to depend functionally on the renormalized indirect correlation function $\tau=h-c-\beta u_1$, i.e., $B(r,\varphi_1,\varphi_2)\equiv B([\tau(r,\varphi_1,\varphi_2)])$. For instance in the case of the SMSA approximation, the bridge function B depends on τ according to Eq. (8). In view of this, it is quite natural to conserve the unique functional dependence of $B_\lambda(r,\varphi_1,\varphi_2)=B[\tau_\lambda(r,\varphi_1,\varphi_2)]$ on $\tau(r,\varphi_1,\varphi_2)$ for any $\lambda\in[0,1]$, where $\tau_\lambda=h_\lambda-c_\lambda-\beta u_{1\lambda}$. This is only possible by setting the scaling dependence $\tau_\lambda=\eta(\lambda)\tau$, where $\eta(\lambda)$ denotes an arbitrary switching function with $\eta(0)=0$ and $\eta(1)=1$, so that $B_\lambda=B([\tau_\lambda])=B([\eta(\lambda)\tau])\equiv B_\lambda([\tau])$. From the topology of integral equations it also follows that if h and c are the solutions to the basic (solvent) AOZ equation [Eq. (5)], the functions $h_\lambda=\eta(\lambda)h$ and $c_\lambda=\eta(\lambda)c$ will automatically satisfy the solute-solvent AOZ equation [Eq. (A5)], making the ratio $h_\lambda/c_\lambda=h/c$ independent of λ. Thus the functional dependence can be conserved if the long-ranged potential is turned on as $u_{1\lambda}=\eta(\lambda)u_1$ using the same switching function. This does not concern, of course, the total potential u_λ which will depend on λ in a more complicated way, $\beta u_\lambda=-\ln[1+\eta(\lambda)h]+\eta(\lambda)(h-c)+B[\eta(\lambda)\tau]$, as follows from Eq. (A7) by solving the inverse AOZ problem (i.e., by reproducing the interparticle potential from a given form of the correlation functions). But this is not important for the current stage of the calculations since the potential u_λ has already been expressed in terms of correlation functions and thus no longer enters into the equation [Eq. (A13)] for the chemical potential. Taking into account the functional scaling behavior yields

$$\int_0^1 \frac{\partial h_\lambda}{\partial\lambda} B_\lambda d\lambda = \frac{h(r,\varphi_1,\varphi_2)}{\tau(r,\varphi_1,\varphi_2)}\int_0^{\tau(r,\varphi_1,\varphi_2)} B(\tau')d\tau', \tag{A14}$$

where for the SMSA bridge function [Eq. (8)] we have

$$\int_0^\tau B(\tau')d\tau' = (1+\tau)\ln(1+\tau)-\frac{\tau(\tau+2)}{2}. \tag{A15}$$

An essential feature of Eq. (A14) is that the scaling function $\eta(\lambda)$ has been canceled, indicating the scale path independence of the λ integration. Additional simplifications in Eq. (A13) are possible by expressing the one- and two-dimensional integrations with respect to angle variables in terms of harmonics coefficients [see Eqs. (14)–(17)]. Then one finds

$$\begin{aligned}\beta\mu^* = {} & \ln Z_0 - 2\ln Z + \beta\sum_{n=1}^{\infty} a_n\xi_{n00} + \rho\int d\mathbf{r} \\ & \times\Bigg[\sum_{n,m,n',m',l}\xi_{nn'l}\xi_{mm'l}\Bigg(\frac{1}{2}h_{nml}(r)[h_{n'm'l}(r)-c_{n'm'l}(r)] \\ & + g_{nml}(r)B_{n'm'l}(r)\Bigg) - \sum_{n,m=0}^{\infty}\xi_{n00}\xi_{m00}c_{nm0}(r) - \frac{1}{(2\pi)^2} \\ & \times\int d\varphi_1 d\varphi_2\xi(\varphi_1)\xi(\varphi_2)\frac{h(r,\varphi_1,\varphi_2)}{\tau(r,\varphi_1,\varphi_2)}\int_0^{\tau(r,\varphi_1,\varphi_2)} B(\tau')d\tau'\Bigg],\end{aligned} \tag{A16}$$

or in the matrix form

$$\begin{aligned}\beta\mu^* = {} & \ln Z_0 - 2\ln Z + \beta\sum_{n=1}^{\infty} a_n\xi_{n00} - \rho\sum_{n,m=0}^{\infty} C_{nm} + \rho \\ & \times\int\frac{d\mathbf{k}}{(2\pi)^3}\sum_{l=0,1}\mathrm{tr}\Bigg(\frac{1}{2}\boldsymbol{\xi}^{(l)}\mathbf{h}^{(l)}(k)[\boldsymbol{\xi}^{(l)}\mathbf{h}^{(l)}(k)-\boldsymbol{\xi}^{(l)}\mathbf{c}^{(l)}(k)] \\ & + \boldsymbol{\xi}^{(l)}\mathbf{g}^{(l)}(k)\boldsymbol{\xi}^{(l)}\mathbf{B}^{(l)}(k)\Bigg) \\ & - \frac{\rho}{(2\pi)^2}\int d\mathbf{r}\, d\varphi_1 d\varphi_2\xi(\varphi_1)\xi(\varphi_2)\frac{h(r,\varphi_1,\varphi_2)}{\tau(r,\varphi_1,\varphi_2)} \\ & \times\int_0^{\tau(r,\varphi_1,\varphi_2)} B(\tau')d\tau',\end{aligned} \tag{A17}$$

where $\mathbf{B}^{(l)}(k)$ is the matrix with the (nm)th elements $B_{nml}(k)$ (for each given $l=0$ and 1) being the Fourier transform of the harmonic coefficients $B_{nml}(r)$ [see Eq. (14)] for the function $B(r,\varphi_1,\varphi_2)$, tr denotes the trace operation, $C_{nm}=\xi_{n00}\xi_{m00}c_{nm0}(k=0)$, and Z_0 can be reduced to the zeroth-order modified Bessel function of the first kind $I_0(\beta H)$. Note that since the correlation functions h and τ enter into the last term of the right-hand side of Eq. (A16) in a very complicated nonlinear way [see Eq. (A15)], the corresponding integration in angle variables for this term cannot be done in quadratures.

In such a way, the chemical potential can be evaluated for anisotropic orientationally (ferromagnetically) ordered systems directly in terms of correlation functions. In the particular case of disordered (paramagnetic) states, when $H=0$ and $\xi(\varphi)=\xi_0(\varphi)=1$ with $\xi_{000}=1$ and $\xi_{nml}=0$ otherwise, as well as $\ln Z_0=\ln Z=0$, $a_n=0$, and the functions h,c,τ, and B do not depend on φ_1 and φ_2, so that $h_{000}=h(r)$, $c_{000}=c(r)$, $\tau_{000}=h(r)$, and $B_{000}=B(r)$, Eq. (A16) completely coincides with that for the excess chemical potential obtained in previous work [8,40,42,43] for isotropic nonmagnetic fluids.

APPENDIX B: HELMHOLTZ FREE ENERGY

The Helmholtz free energy per particle can be reproduced using the thermodynamic relation $\mathcal{F}/N=\mu-P/\rho$ and known values of P and μ. Alternatively, it can be calculated directly in terms of correlation functions, similarly to what has been done already for the chemical potential. To accomplish this, let us consider now our system in a situation where the interaction between all of the particles varies according to the λ-dependent potential $u_\lambda(r,\varphi_1,\varphi_2)$ from $u_{\lambda=0}=0$ to $u_{\lambda=1}=u(r,\varphi_1,\varphi_2)$. An auxiliary external potential $V_\lambda(\varphi)$ in the presence of the primary field H is introduced to keep the one-body distribution function of each particle fixed (despite the variation of the two-body potential u_λ) and equal to the function $\xi(\varphi)$ corresponding to the basic state of the system at $\lambda=1$ (so that $V_{\lambda=1}=0$). The partition function of the system related to the above λ state reads

$$\mathcal{Q}_N(\lambda)=\int \frac{d\mathbf{q}^N}{N!\,\Lambda^{3N}}\exp\left[-\beta\left(\sum_{i=1}^{N}[H\cos(\varphi_i)+V_\lambda(\varphi_i)]+\sum_{i<j}^{N}u_\lambda(r_{ij},\varphi_i,\varphi_j)\right)\right]\equiv\int\frac{d\mathbf{q}^N}{N!\,\Lambda^{3N}}\exp[-\beta U_\lambda(\mathbf{q}^N)] \tag{B1}$$

[note that $\mathcal{Q}_N(\lambda=1)=\mathcal{Q}_N(V,T,H)$; see Eq. (A1)]. The differentiation of $\mathcal{F}(\lambda)=-k_BT\ln\mathcal{Q}_N(\lambda)$ gives

$$\frac{\partial\mathcal{F}(\lambda)}{\partial\lambda}=N\left\langle\frac{\partial V_\lambda}{\partial\lambda}\right\rangle_\lambda+\left\langle\sum_{i<j}^{N}\frac{\partial u_\lambda(r_{ij},\varphi_i,\varphi_j)}{\partial\lambda}\right\rangle_\lambda, \tag{B2}$$

where now

$$\langle\cdots\rangle_\lambda=[1/N!\,\Lambda^{3N}\mathcal{Q}_N(\lambda)]\int\cdots d\mathbf{q}^N\exp[-\beta U_\lambda(\mathbf{q}^N)].$$

Then taking into account the equality $\mathcal{F}\equiv\mathcal{F}(1)=\mathcal{F}(0)+\int_0^1 d\lambda\;\partial\mathcal{F}(\lambda)/\partial\lambda$, one finds

$$\frac{\mathcal{F}}{N}=\frac{\mathcal{F}^{(0)}}{N}+W+\frac{1}{2}\frac{\rho}{(2\pi)^2}\int_0^1 d\lambda\int d\mathbf{r}\,d\varphi_1 d\varphi_2\times\xi(\varphi_1)\xi(\varphi_2)g(\lambda,r,\varphi_1,\varphi_2)\frac{\partial u_\lambda(r,\varphi_1,\varphi_2)}{\partial\lambda}, \tag{B3}$$

where

$$W=(1/2\pi)\int_0^1 d\lambda\int d\varphi\;\xi(\varphi)\,\partial V_\lambda(\varphi)/\partial\lambda=(1/2\pi)\int d\varphi\;\xi(\varphi)V(\varphi)$$

with $V=-V_{\lambda=0}$, and $\mathcal{F}^{(0)}\equiv\mathcal{F}(0)=-k_BT\ln\mathcal{Q}_N(\lambda=0)=Nk_BT[\ln(\rho\Lambda^3)-1-\ln Z]$ is the free energy in the absence of interparticle interactions (but in the presence of external fields H and V).

In view of Eqs. (5), (6), and (10), the AOZ, closure, and LMBW equations corresponding to the λ state take the forms

$$h(\lambda,r,\varphi_1,\varphi_2)=c(\lambda,r,\varphi_1,\varphi_2)+\frac{\rho}{2\pi}\int_V d\mathbf{r}'\int_0^{2\pi}d\varphi\;\xi(\varphi)\times c(\lambda,|\mathbf{r}-\mathbf{r}'|,\varphi_1,\varphi)h(\lambda,r',\varphi,\varphi_2), \tag{B4}$$

$$g(\lambda,r,\varphi_1,\varphi_2)=\exp[-\beta u_\lambda(r,\varphi_1,\varphi_2)+h(\lambda,r,\varphi_1,\varphi_2)-c(\lambda,r,\varphi_1,\varphi_2)+B(\lambda,r,\varphi_1,\varphi_2)], \tag{B5}$$

and

$$\frac{d}{d\varphi}\ln\xi(\varphi)=\frac{d}{d\varphi}\beta H\cos\varphi-\frac{d\beta V_\lambda(\varphi)}{d\varphi}+\frac{\rho}{2\pi}\int_V d\mathbf{r}\int_0^{2\pi}d\varphi' c(\lambda,r,\varphi,\varphi')\frac{d\xi(\varphi')}{d\varphi'}, \tag{B6}$$

respectively. In order to avoid confusion, it is worth stressing that the correlation functions $g(\lambda,r,\varphi_1,\varphi_2)=h(\lambda,r,\varphi_1,\varphi_2)+1$, $c(\lambda,r,\varphi_1,\varphi_2)$, and $B(\lambda,r,\varphi_1,\varphi_2)$ are related to the λ state of the whole system. They have nothing to do with correlation functions $g_\lambda(r,\varphi_1,\varphi_2)=h_\lambda(r,\varphi_1,\varphi_2)+1$, $c_\lambda(r,\varphi_1,\varphi_2)$, and $B_\lambda(r,\varphi_1,\varphi_2)$ introduced earlier (see Appendix A) to describe the λ state of a separate particle. Because of this, the λ integration in Eq. (B3) will lead to different results in comparison with those corresponding to Eq. (A11), despite the fact that both formulas are similar. Indeed, taking the partial derivative $\partial u_\lambda(r,\varphi_1,\varphi_2)/\partial\lambda$ from Eq. (B5) we come to an expression similar to Eq. (A8). After substituting it into Eq. (B3) and performing the λ integration, this will give the same result for the first terms $h^2/2-c+B$ corresponding to exact differentials, because the boundary conditions at $\lambda=0$ and 1 are the same for both of the above sets of correlation functions, i.e., $\{h,c,B\}_{\lambda=0}=0=\{h,c,B\}(\lambda=0)$ and

$$\{h,c,B\}_{\lambda=1}(r,\varphi_1,\varphi_2)=\{h,c,B\}(\lambda=1,r,\varphi_1,\varphi_2)=\{h,c,B\}(r,\varphi_1,\varphi_2).$$

Because of this we have also that $W=w$ [see Eqs. (A9) and (B6)]. But for a given $u_\lambda(r,\varphi_1,\varphi_2)$, both of the sets differ in their values for the correlation functions at intermediate states $\lambda\in]0,1[$. For this reason, when handling the term $h(\lambda,r,\varphi_1,\varphi_2)\,\partial c(\lambda,r,\varphi_1,\varphi_2)/\partial\lambda$ we can no longer use the equality [Eq. (A12)] which now is not valid, because the (solute-solvent) AOZ equation [Eq. (A5)] differs from the (system) AOZ equation [Eq. (B4)]. The latter can be rewritten in k space in matrix form as

$$\mathbf{h}^{(l)}(\lambda,k)=\mathbf{c}^{(l)}(\lambda,k)+\rho\mathbf{c}^{(l)}(\lambda,k)\boldsymbol{\xi}^{(l)}\mathbf{h}^{(l)}(\lambda,k), \tag{B7}$$

where $\mathbf{h}^{(l)}(\lambda,k)$ and $\mathbf{c}^{(l)}(\lambda,k)$ denote the square matrices with the (nm) elements $h_{nml}(\lambda,k)$ and $c_{nml}(\lambda,k)$, respectively, for each $l=0$ or 1, with $h_{nml}(\lambda,k)$ and $c_{nml}(\lambda,k)$ being the Fourier transform of the planar harmonic coefficients [Eq. (14)] for the functions $h(\lambda,r,\varphi_1,\varphi_2)$ and $c(\lambda,r,\varphi_1,\varphi_2)$. From Eq. (B7) it is easy to show that the matrices $\mathbf{h}^{(l)}$ and $\mathbf{c}^{(l)}$ satisfy

$$[\mathbf{I}+\rho\boldsymbol{\xi}^{(l)}\mathbf{h}^{(l)}(\lambda,k)]^{-1}=\mathbf{I}-\rho\boldsymbol{\xi}^{(l)}\mathbf{c}^{(l)}(\lambda,k). \tag{B8}$$

Then using the matrix identity $\partial \ln\det\mathbf{M}/\partial\lambda=\mathrm{tr}(\mathbf{M}^{-1}\partial\mathbf{M}/\partial\lambda)$, where det denotes the determinant operation, we have for matrix $\mathbf{M}(\lambda,k)=\mathbf{I}+\rho\boldsymbol{\xi}^{(l)}\mathbf{h}^{(l)}(\lambda,k)$ in view of Eq. (B8) that

$$\frac{\partial}{\partial\lambda}\ln\det\mathbf{M}=\mathrm{tr}\left([\mathbf{I}-\rho\boldsymbol{\xi}^{(l)}\mathbf{c}^{(l)}(\lambda,k)]\rho\frac{\partial\boldsymbol{\xi}^{(l)}\mathbf{h}^{(l)}}{\partial\lambda}\right) \tag{B9}$$

and thus

$$\mathrm{tr}\left(\rho^2\boldsymbol{\xi}^{(l)}\mathbf{c}^{(l)}(\lambda,k)\frac{\partial\boldsymbol{\xi}^{(l)}\mathbf{h}^{(l)}(\lambda,k)}{\partial\lambda}\right)=\frac{\partial}{\partial\lambda}\{\mathrm{tr}[\rho\boldsymbol{\xi}^{(l)}\mathbf{h}^{(l)}(\lambda,k)]-\ln\det[\mathbf{I}+\rho\boldsymbol{\xi}^{(l)}\mathbf{h}^{(l)}(\lambda,k)]\}. \tag{B10}$$

Taking into account that $-h\partial c/\partial\lambda=-\partial(hc)/\partial\lambda+c\partial h/\partial\lambda$ we obtain for the last term, which appears in the λ integrand in the right-hand side of Eq. (B3), that

$$\begin{aligned}\int d\mathbf{r}\,d\varphi_1 d\varphi_2\xi(\varphi_1)\xi(\varphi_2)c(\lambda,r,\varphi_1,\varphi_2)\frac{\partial h(\lambda,r,\varphi_1,\varphi_2)}{\partial\lambda}&=\int\frac{d\mathbf{k}}{(2\pi)^3}d\varphi_1 d\varphi_2\xi(\varphi_1)\xi(\varphi_2)c(\lambda,k,\varphi_1,\varphi_2)\frac{\partial h(\lambda,k,\varphi_1,\varphi_2)}{\partial\lambda}\\&=\int\frac{d\mathbf{k}}{(2\pi)^3}\mathrm{tr}\left(\boldsymbol{\xi}^{(l)}\mathbf{c}^{(l)}(\lambda,k)\frac{\partial\boldsymbol{\xi}^{(l)}\mathbf{h}^{(l)}(\lambda,k)}{\partial\lambda}\right)\end{aligned} \tag{B11}$$

which, in view of Eq. (B10), presents an exact differential and can easily be integrated. Thus, Eq. (B3) becomes

$$\begin{aligned}\frac{\beta\mathcal{F}}{N}=\frac{\beta\mathcal{F}_0}{N}+2(\ln Z_0-\ln Z)+\beta\sum_{n=1}^{\infty}a_n\xi_{n00}-\frac{\rho}{2}&\times\sum_{n,m=0}^{\infty}C_{nm}+\frac{\rho}{2}\sum_{l=0,1}\int\frac{d\mathbf{k}}{(2\pi)^3}\\&\times\left\{\mathrm{tr}\left[\boldsymbol{\xi}^{(l)}\mathbf{h}^{(l)}(k)\left(\frac{1}{2}\boldsymbol{\xi}^{(l)}\mathbf{h}^{(l)}(k)-\boldsymbol{\xi}^{(l)}\mathbf{c}^{(l)}(k)\right)\right]\right.\\&+\frac{1}{\rho^2}\{\mathrm{tr}[\rho\boldsymbol{\xi}^{(l)}\mathbf{h}^{(l)}(k)]-\ln\det[\mathbf{I}+\rho\boldsymbol{\xi}^{(l)}\mathbf{h}^{(l)}(k)]\}\\&\left.+\int_0^1 d\lambda\,\boldsymbol{\xi}^{(l)}\mathbf{g}^{(l)}(\lambda,k)\frac{\partial\boldsymbol{\xi}^{(l)}\mathbf{B}^{(l)}(\lambda,k)}{\partial\lambda}\right\},\end{aligned} \tag{B12}$$

where $\beta\mathcal{F}_0/N=\ln(\rho\Lambda^3)-1-\ln Z_0$ is the free energy per particle of an interacting system in the presence of an external field H. The last term in Eq. (B12) must be approximated. It cannot be integrated analytically using the scaling formalism as this has been done when considering the bridge contribution to the chemical potential [see Eq. (A14)]. The reason is that now the ratio $h(\lambda,r,\varphi_1,\varphi_2)/c(\lambda,r,\varphi_1,\varphi_2)$ cannot be made independent of λ due to the differences in the AOZ equations (A5) and (B4). For the HNC approximation, the last term can be neglected. For other closures, including the SMSA, the integration with the bridge function should be performed numerically using correlation functions obtained from the integral equation theory at intermediate λ states.

[1] N. E. Frankel and C. J. Thompson, J. Phys. C **8**, 3194 (1975).
[2] P. C. Hemmer and D. Imbro, Phys. Rev. A **16**, 380 (1977).
[3] J. M. Tavares, M. M. Telo da Gama, P. I. C. Teixeira, J. J. Weis, and M. J. P. Nijmeijer, Phys. Rev. E **52**, 1915 (1995).
[4] F. Schinagl, H. Iro, and R. Folk, Eur. Phys. J. B **8**, 113 (1999).
[5] F. Schinagl, R. Folk, and H. Iro, Condens. Matter Phys. **2**, 313 (1999).
[6] W. Fenz and R. Folk, Phys. Rev. E **67**, 021507 (2003).
[7] W. Fenz, R. Folk, I. M. Mryglod, and I. P. Omelyan, Phys. Rev. E **68**, 061510 (2003).
[8] I. P. Omelyan, I. M. Mryglod, R. Folk, and W. Fenz, Phys. Rev. E **69**, 061506 (2004).
[9] E. Lomba, J. J. Weis, N. G. Almarza, F. Bresme, and G. Stell, Phys. Rev. E **49**, 5169 (1994).
[10] F. Lado and E. Lomba, Phys. Rev. Lett. **80**, 3535 (1998).
[11] T. G. Sokolovska, Physica A **253**, 459 (1998).
[12] F. Lado, E. Lomba, and J. J. Weis, Phys. Rev. E **58**, 3478 (1998).
[13] T. G. Sokolovska and R. O. Sokolovskii, Phys. Rev. E **59**, R3819 (1999).
[14] E. Lomba, F. Lado, and J. J. Weis, Condens. Matter Phys. **4**, 45 (2001).
[15] T. G. Sokolovska, R. O. Sokolovskii, and M. F. Holovko, Phys. Rev. E **62**, 6771 (2000).
[16] I. P. Omelyan, W. Fenz, I. M. Mryglod, and R. Folk, Phys. Rev. Lett. **94**, 045701 (2005).
[17] M. J. P. Nijmeijer and J. J. Weis, Phys. Rev. E **53**, 591 (1996).
[18] M. J. P. Nijmeijer and J. J. Weis, in *Annual Review of Computational Physics IV*, edited by D. Stauffer (World Scientific, Singapore, 1996).
[19] J. J. Weis, M. J. P. Nijmeijer, J. M. Tavares, and M. M. Telo da Gama, Phys. Rev. E **55**, 436 (1997).
[20] M. J. P. Nijmeijer, A. Parola, and L. Reatto, Phys. Rev. E **57**, 465 (1998).
[21] I. M. Mryglod, I. P. Omelyan, and R. Folk, Phys. Rev. Lett. **86**, 3156 (2001).
[22] D. J. Tulimieri, J. Yoon, and M. H. W. Chan, Phys. Rev. Lett. **82**, 121 (1999).
[23] K. Moon and S. M. Girvin, Phys. Rev. Lett. **75**, 1328 (1995).
[24] N. B. Wilding, F. Schmid, and P. Nielaba, Phys. Rev. E **58**, 2201 (1998).
[25] G. Kahl, E. Schöll-Paschinger, and A. Lang, Monatsch. Chem. **132**, 1413 (2001).
[26] E. Schöll-Paschinger, D. Levesque, J. J. Weis, and G. Kahl, Phys. Rev. E **64**, 011502 (2001).
[27] G. Kahl, E. Schöll-Paschinger, and G. Stell, J. Phys.: Condens. Matter **14**, 9153 (2002).
[28] O. Antonevych, F. Forstmann, and E. Diaz-Herrera, Phys. Rev.

E **65**, 061504 (2002).
[29] E. Schöll-Paschinger and G. Kahl, J. Chem. Phys. **118**, 7414 (2003).
[30] D. Pini, M. Tau, A. Parola, and L. Reatto, Phys. Rev. E **67**, 046116 (2003).
[31] N. B. Wilding, Phys. Rev. E **67**, 052503 (2003).
[32] R. O. Sokolovskii, Phys. Rev. B **61**, 36 (2000).
[33] S. Romano and R. O. Sokolovskii, Phys. Rev. B **61**, 11379 (2000).
[34] M. Blume, V. J. Emery, and R. B. Griffiths, Phys. Rev. A **4**, 1071 (1971).
[35] A. Maciolek, M. Krech, and S. Dietrich, Phys. Rev. E **69**, 036117 (2004).
[36] J. P. Hansen and I. R. McDonald, *Theory of Simple Liquids*, 2nd ed. (Academic, London, 1986).
[37] R. Lovett, C. Y. Mou, and F. P. Buff, J. Chem. Phys. **65**, 570 (1976).
[38] M. S. Wertheim, J. Chem. Phys. **65**, 2377 (1976).
[39] C. G. Gray and K. E. Gubbins, *Theory of Molecular Fluids* (Clarendon, Oxford, 1984), Vol. 1.
[40] N. Choudhury and S. K. Ghosh, J. Chem. Phys. **116**, 8517 (2002).
[41] J. G. Kirkwood, J. Chem. Phys. **3**, 300 (1935).
[42] A. Kovalenko and F. Hirata, Chem. Phys. Lett. **349**, 496 (2001).
[43] A. Kovalenko and F. Hirata, J. Chem. Phys. **110**, 10095 (1999).
[44] J. S. Høye, J. L. Lebowitz, and G. Stell, J. Chem. Phys. **61**, 3253 (1974).
[45] A. Kovalenko, S. Ten-no, and F. Hirata, J. Comput. Chem. **20**, 928 (1999).
[46] B. C. Eua and K. Rah, J. Chem. Phys. **111**, 3327 (1999).
[47] A. Z. Panagiotopoulos, Mol. Simul. **9**, 1 (1992).
[48] A. M. Ferrenberg and R. H. Swendsen, Phys. Rev. Lett. **61**, 2635 (1988); **63**, 1195 (1989).
[49] K. Binder, Rep. Prog. Phys. **60**, 487 (1997).
[50] P. H. E. Meijer, M. Keskin, and I. L. Pegg, J. Chem. Phys. **88**, 1976 (1988).
[51] B. Groh and S. Dietrich, Phys. Rev. Lett. **72**, 2422 (1994).
[52] P. H. von Konynenburg and R. L. Scott, Philos. Trans. R. Soc. London, Ser. A **298**, 495 (1980).
[53] J. Zinn-Justin, *Quantum Field Theory and Critical Phenomena* (Clarendon, Oxford, 1983).
[54] S. M. Kast, Phys. Rev. E **67**, 041203 (2003).